in Fig. 3. The distribution of ^{125}I-IATP to blood cells was significantly decreased by CA inhibitors (acetazolamide and chlorthalidone), but not by chlorpromazine or phenothiazine. The distribution of ^{125}I-IMTP to blood cells was not affected by any of the compounds used in the present study.

4. Discussion

In the present study, we synthesized a methyl sulfone-type COX-2 inhibitor, 5-(4-iodophenyl)-1-[4-(methylsulfonyl)phenyl]-3-trifluoromethyl-1*H*-pyrazole (IMTP). The potential of radioiodinated IMTP for imaging COX-2 expression was evaluated in comparison with a ^{125}I-labeled celecoxib analogue with a sulfonamide moiety (^{125}I-IATP). The major findings in the present study can be summarized as follows: (1) IMTP had a high inhibitory potency and selectivity for COX-2. (2) ^{125}I-IMTP showed a biodistribution compatible with the known distribution of COX-2. (3) The blood clearance of ^{125}I-IMTP was much faster than that of ^{125}I-IATP. (4) ^{125}I-IATP showed markedly higher distribution to blood cells than ^{125}I-IMTP, which was decreased by CA inhibitors. These results demonstrate that the substitution of the sulfonamide moiety to a methyl sulfone moiety effectively improved the blood clearance of the compound, indicating the loss of the cross reactivity with CA in ^{125}I-IMTP. Methyl sulfone-type COX-2 inhibitors may be a preferential candidate as radiopharmaceuticals for COX-2 expression.

The methyl sulfone moiety and sulfonamide moiety at position 4 of the 1-phenyl ring are considered to be optimal for COX-2 selectivity [11]. In this regard, several COX-2 inhibitors with a methyl sulfone or sulfonamide moiety were recently radiolabeled and preliminarily evaluated as imaging agents [12–14,16]. However, the effects of these moieties on the pharmacokinetics of the labeled tracers have not been determined. Our results clearly showed that the substitution of the sulfonamide moiety to the methyl sulfone moiety effectively improved the blood clearance of the compound (Fig. 2). In addition, the high distribution of ^{125}I-IATP to blood cells was significantly inhibited by CA inhibitors (Fig. 3). Recently, it was reported that sulfonamide-type celecoxib analogues show high affinity to carbonic anhydrase (CA) [18]. Agents containing sulfonamides (e.g., acetazolamide) have been widely used in clinical medicine to inhibit carbonic anhydrase (CA) [17,18]. The slow blood clearance of ^{125}I-IATP can be ascribed to the affinity of its sulfonamide moiety to CA in erythrocytes [17,18]. These results indicate the feasibility of methyl sulfone-type COX-2 inhibitors as radiopharmaceuticals for COX-2 expression.

Although COX-2 is an inducible isoform, it is predominantly found in the normal brain and kidneys [20]. The preferential uptakes of ^{125}I-IMTP and ^{125}I-IATP in these organs were compatible with the expression of COX-2 in these organs. The high brain-to-blood ratio of ^{125}I-IMTP indicates the feasibility of this compound for COX-2 imaging in the brain. On the other hand, no marked ^{125}I-IMTP accumulation was observed in the stomach or thyroid, indicating its stability to in vivo deiodination. The present results using ^{125}I-IMTP are consistent with those using ^{18}F-SC-58125, which showed preferential uptakes in the brain and kidneys with rapid blood clearance [12]. SC-58125 is a methyl sulfone-type COX-2 inhibitor that has the same structure as IMTP except that the fluorine in SC-58125 is replaced with iodine in IMTP. These results further confirm the potentials of methyl sulfone-type COX-2 inhibitors as radiopharmaceuticals for COX-2 expression.

In the present study, we determined the biodistribution of the labeled compounds at several time points within 3 h, considering that small animals generally show rapid pharmacokinetics compared with that in humans. Consequently, we demonstrated that ^{125}I-IMTP showed preferential uptakes in the brain and kidneys with much faster blood clearance than ^{125}I-IATP. Time points <3 h appear to be appropriate to extrapolate the pharmacokinetics in humans from those in rats. We generally perform experiments to block the uptake of a candidate compound in tissues by coinjecting the nonradioactive compound, in order to confirm its specific distribution. In the present study, however, we did not perform such blocking experiments, because the physiological expression levels of COX-2 are relatively low compared with those in the pathological state. Such blocking experiments do not appear to be suitable to demonstrate the specific distribution of radiolabeled COX-2 inhibitors. McCarthy et al. [12] failed to obtain in vivo blocking data to show the specific binding of a radiotracer (^{18}F-SC58125) to COX-2 in rats. Contrarily, de Vries et al. [13] indicated the specific binding of ^{18}F-desbromo-DuP-697 by blocking experiments in rats. Experiments in animal models with higher COX-2 expression may be necessary to assess the specific binding of tracers to COX-2. We must await further studies to achieve this goal. Experiments to demonstrate the advantage of longer half-lives of SPECT nuclides are also required.

The COX-2 inhibitory potency of IMTP and IATP was higher than that of meloxicam and was comparable to that of SC-58125, suggesting that the introduction of iodine at position 4 of the 5-phenyl ring did not largely affect the COX-2 inhibitory potency. In addition, IC_{50} ratios (COX-1/COX-2) for IMTP and IATP showed high isoform selectivity of these compounds for COX-2 (Table 1), indicating that the selectivity of IMTP and IATP for COX-2 is comparable to celecoxib [21,22]. These results were consistent with the consideration on the structure–activity relationship reported by Herschman et al. [11] and suggest that the introduction of iodine at position 4 of the 5-phenyl ring is acceptable.

5. Conclusion

A radioiodinated COX-2 inhibitor, ^{125}I-IMTP, was synthesized. Our results showed a high inhibitory potency

and selectivity of IMTP for COX-2. In addition, radioiodinated-IMTP was stable for in vivo deiodination and showed rapid blood clearance. These results indicate that radioiodinated IMTP, a methyl sulfone-type COX-2 inhibitor, meets the basic requirements for an effective radiopharmaceutical and deserves further elucidation as a SPECT radiopharmaceutical for imaging COX-2 expression.

Acknowledgments

This study was supported in part by Grants-in-Aid for General Scientific Research from the Ministry of Education, Culture, Sports, Science and Technology of Japan. The authors wish to thank Dr. H Hashimoto of Chemical Research Laboratories, Japan Tobacco, Inc., for useful discussion.

References

[1] Davies NM, Good RL, Roupe KA, Yancz JA. Cyclooxygenase-3: axiom, dogma, anomaly, enigma or splice error?—Not as easy as 1, 2, 3. J Pharm Pharm Sci 2004;7:217–26.

[2] FitzGerald GA. COX-2 and beyond: approaches to prostaglandin inhibition in human disease. Nat Rev Drug Discov 2003;2:879–90.

[3] Collaco-Moraes Y, Aspey B, Harrison M, de-Belleroche J. Cyclo-oxygenase-2 messenger RNA induction in focal cerebral ischemia. J Cereb Blood Flow Metab 1996;16:1366–72.

[4] Nogawa S, Zhang F, Ross ME, Iadecola C. Cyclo-oxygenase-2 gene expression in neurons contributes to ischemic brain damage. J Neurosci 1997;17:2746–55.

[5] Hara K, Kong DL, Sharp FR, Weinstein PR. Effect of selective inhibition of cyclooxygenase 2 on temporary focal cerebral ischemia in rats. Neurosci Lett 1998;256:53–6.

[6] Yokota C, Inoue H, Kuge Y, Abumiya T, Tagaya M, Hasegawa Y, et al. Cyclooxygenase-2 expression associated with spreading depression in a primate model. J Cereb Blood Flow Metab 2003;23:395–8.

[7] Yokota C, Kuge Y, Inoue H, Tagaya M, Kito G, Susumu T, et al. Post-ischemic cyclooxygenase-2 expression is regulated by the extent of cerebral blood flow reduction in non-human primates. Neurosci Lett 2003;341:37–40.

[8] Yokota C, Kaji T, Kuge Y, Inoue H, Tamaki N, Minematsu K. Temporal and topographic profiles of cyclooxygenase-2 expression during 24 h of focal brain ischemia in rats. Neurosci Lett 2004; 357:219–22.

[9] Yokota C, Kuge Y, Inoue H, Tamaki N, Minematsu K. Bilateral induction of the S-100A9 gene in response to spreading depression is modulated by the cyclooxygenase-2 activity. J Neurol Sci 2005;234: 11–6.

[10] Kaji T, Kuge Y, Yokota C, Tagaya M, Inoue H, Shiga T, et al. Characterisation of [^{123}I]iomazenil distribution in a rat model of focal cerebral ischaemia in relation to histopathological findings. Eur J Nucl Med Mol Imaging 2004;31:64–70.

[11] Herschman HR, Talley JJ, DuBois R. Cyclooxygenase 2 (COX-2) as a target for therapy and noninvasive imaging. Mol Imaging Biol 2003; 5:286–303.

[12] McCarthy TJ, Sheriff AU, Graneto MJ, Talley JJ, Welch MJ. Radiosynthesis, in vitro validation, and in vivo evaluation of ^{18}F-labeled COX-1 and COX-2 inhibitors. J Nucl Med 2002;43:117–24.

[13] de Vries EF, van Waarde A, Buursma AR, Vaalburg W. Synthesis and in vivo evaluation of ^{18}F-desbromo-DuP-697 as a PET tracer for cyclooxygenase-2 expression. J Nucl Med 2003;44:1700–6.

[14] Wust FR, Hohne A, Metz P. Synthesis of ^{18}F-labelled cyclo-oxygenase-2 (COX-2) inhibitors via Stille reaction with 4-[^{18}F]fluoroiodobenzene as radiotracers for positron emission tomography (PET). Org Biomol Chem 2005;3:503–7.

[15] Yang DJ, Bryant J, Chang JY, Mendez R, Oh CS, Yu DF, et al. Assessment of cyclooxygense-2 expression with ^{99m}Tc-labeled celebrex. Anticancer Drugs 2004;15:255–63.

[16] Kabalka GW, Mereddy AR, Schuller HM. Synthesis of an iodine-123-labeled celecoxib analogue: a potential SPECT agent. J Label Compd Radiopharm 2005;48:295–300.

[17] Boddy A, Edwards P, Rowland M. Binding of sulfonamides to carbonic anhydrase: influence on distribution within blood and on pharmacokinetics. Pharm Res 1989;6:203–9.

[18] Weber A, Casini A, Heine A, Kuhn D, Supuran CT, Scozzafava A, et al. Unexpected nanomolar inhibition of carbonic anhydrase by COX-2-selective celecoxib: new pharmacological opportunities due to related binding site recognition. J Med Chem 2004;47:550–7.

[19] Kiyono Y, Kanegawa N, Kawashima H, Kitamura Y, Iida Y, Saji H. Evaluation of radioiodinated (*R*)-*N*-methyl-3-(2-iodophenoxy)-3-phenylpropanamine as a ligand for brain norepinephrine transporter imaging. Nucl Med Biol 2004;31:147–53.

[20] Kam PC, See AU. Cyclo-oxygenase isoenzymes: physiological and pharmacological role. Anaesthesia 2000;55:442–9.

[21] Warner TD, Giuliano F, Vojnovic I, Bukasa A, Mitchell JA, Vane JR. Nonsteroid drug selectivities for cyclo-oxygenase-1 rather than cyclo-oxygenase-2 are associated with human gastrointestinal toxicity: a full in vitro analysis. Proc Natl Acad Sci U S A 1999;96:7563–8.

[22] Kato M, Nishida S, Kitasato H, Sakata N, Kawai S. Cyclooxygenase-1 and cyclooxygenase-2 selectivity of non-steroidal anti-inflammatory drugs: investigation using human peripheral monocytes. J Pharm Pharmacol 2001;53:1679–85.

ARTICLES

Development of a Rhenium-186-Labeled MAG3-Conjugated Bisphosphonate for the Palliation of Metastatic Bone Pain Based on the Concept of Bifunctional Radiopharmaceuticals

Kazuma Ogawa,[†,‡,§] Takahiro Mukai,[†,∥] Yasushi Arano,[⊥] Masahiro Ono,[†] Hirofumi Hanaoka,[†] Seigo Ishino,[†] Kazuyuki Hashimoto,[#] Hiroshi Nishimura,[§] and Hideo Saji*[,†]

Department of Patho-Functional Bioanalysis, Graduate School of Pharmaceutical Sciences, Kyoto University, Yoshida Shimoadachi-cho, Sakyo-ku, Kyoto 606-8501, Japan, Central Institute of Radioisotopes Science, Division of Tracer Kinetics, Advanced Science Research Center, Kanazawa University, 13-1 Takara-machi, Kanazawa 920-8640, Japan, Radioisotope Laboratory, Kyoto Prefectural University of Medicine, 465 Kajii-cho, Kamigyo-ku, Kyoto 602-0841, Japan, Department of Biomolecular Recognition Chemistry, Graduate School of Pharmaceutical Sciences, Kyushu University, 3-1-1 Maidashi, Higashi-ku, Fukuoka 812-8582, Japan, Department of Molecular Imaging and Radiotherapy, Graduate School of Pharmaceutical Sciences, Chiba University, 1-8-1 Inohana, Chuo-ku, Chiba 260-8675, Japan, and Japan Atomic Energy Research Institute, Tokai-mura, Ibaraki 319-1195, Japan. Received July 10, 2004; Revised Manuscript Received May 20, 2005

Rhenium-186-1-hydroxyethylidene-1,1-diphosphonate (^{186}Re-HEDP) has been used for the palliation of metastatic bone pain. Delayed blood clearance and high gastric uptake of radioactivity have been observed upon injection, due to the instability of ^{186}Re-HEDP in vivo. In this study, on the basis of the concept of bifunctional radiopharmaceuticals, we designed a stable ^{186}Re-mercaptoacetylglycylglycylglycine (MAG3) complex-conjugated bisphosphonate, [[[[(4-hydroxy-4,4-diphosphonobutyl)carbamoylmethyl]carbamoylmethyl]carbamoylmethyl]carbamoylmethanethiolate]oxorhenium(V) (^{186}Re-MAG3-HBP). As a precursor, [1-hydroxy-1-phosphono-4-[2-[2-[2-(2-tritylmercaptoacetylamino)acetylamino]acetylamino]acetylamino]butyl]phosphonic acid (Tr-MAG3-HBP) was synthesized by the conjugation of *N*-[(tritylmercapto)acetyl]glycylglycylglycine (Tr-MAG3) with the bisphosphonate analogue. After deprotection of the trityl group of Tr-MAG3-HBP, ^{186}Re-labeling was performed by reacting $^{186}ReO_4^-$ with $SnCl_2$ in citrate buffer. After purification by HPLC, ^{186}Re-MAG3-HBP showed a radiochemical purity of over 95%. To compare the stability of ^{186}Re-MAG3-HBP and ^{186}Re-HEDP, these ^{186}Re complexes were incubated in phosphate buffer. No measurable decomposition of ^{186}Re-MAG3-HBP occurred over a 24-h period, while only approximately 30% of ^{186}Re-HEDP remained intact 24 h postincubation. In biodistribution experiments, the radioactivity level of ^{186}Re-MAG3-HBP in bone was significantly higher than that of ^{186}Re-HEDP. Blood clearance of ^{186}Re-MAG3-HBP was faster than that of ^{186}Re-HEDP. In addition, the gastric accumulation of ^{186}Re-MAG3-HBP radioactivity was lower than that of ^{186}Re-HEDP. In conclusion, ^{186}Re-MAG3-HBP is expected to be a useful radiopharmaceutical for the palliation of metastatic bone pain.

INTRODUCTION

Malignant tumors, especially breast and prostate carcinomas, frequently metastasize to the bone (*1*). A prominent symptom caused by these metastases is pain, which has a significant impact on the patients' quality of life. Localized radiation therapy is an effective method for the treatment of bone pain (*2*); however, a common problem in patients with bone metastases is the development of multiple sites of metastasis, and so internal radiotherapy using specifically localized beta emitters is preferable. Recently, $^{89}SrCl_2$ has been used as a palliative agent for painful osseous metastases (*3*, *4*). However, ^{89}Sr is a pure beta emitter and has a relatively long half-life (50.5 d). These physical properties could be a disadvantage for clinical use.

Rhemium-186-1-hydroxyethylidene-1,1-diphosphonate (^{186}Re-HEDP) has also been proposed for the palliation of metastatic bone pain (*5*–*7*). ^{186}Re is a Group VII metal that decays with the emission of a beta particle with a maximal energy of 1.07 MeV. A 9% abundance gamma ray with energy of 137 keV is also produced in the decay process, enabling correlative imaging to be performed. Its relatively short physical half-life of 90.6 h accounts for high dose rates and allows for repeated treatments at short time intervals. Moreover, problems of radioactive waste handling and storage are

* To whom correspondence should be addressed. Telephone: 81-75-753-4556; fax: 81-75-753-4568; e-mail: hsaji@pharm.kyoto-u.ac.jp.
† Kyoto University.
‡ Kanazawa University.
§ Kyoto Prefectural University of Medicine.
∥ Kyushu University.
⊥ Chiba University.
Japan Atomic Energy Research Institute.

10.1021/bc040249w CCC: $30.25
Published on Web 07/01/2005

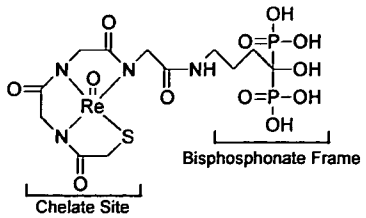

Figure 1. Chemical structure of Re-MAG3-HBP.

reduced. However, ^{186}Re-HEDP has showed delayed blood clearance and high gastric uptake. It has been reported that the unnecessary radiation in patients is due to the poor stability of the ^{186}Re complex in vivo leading to the generation of $^{186}ReO_4^-$ (*8*–*10*). Furthermore, a marked accumulation in bone is also a definitive requirement for a therapeutic drug in the palliation of metastatic bone pain. The accumulation of bisphosphonate analogues in the bone is responsible for the binding of hydroxyl groups of their phosphonate group to Ca^{2+} of hydroxyapatite (*11*). In the case of ^{186}Re-HEDP, since it is reasonable that some hydroxyl groups of HEDP bind to Ca^{2+} of hydroxyapatite and the rest coordinate rhenium, it is predictable that the coordination will reduce the inherent accumulation in bone of HEDP.

Thus, we planned the development of a novel ^{186}Re-labeled compound with a high affinity for bone and low accumulation of radioactivity in other organs. For this purpose, on the basis of the concept of bifunctional radiopharmaceuticals, we designed a stable ^{186}Re-mercaptoacetylglycylglycylglycine (MAG3) complex-conjugated bisphosphonate, [[[[(4-hydroxy-4,4-diphosphonobutyl)carbamoylmethyl]carbamoylmethyl]carbamoylmethyl]carbamoylmethanethiolate]oxorhenium(V) (^{186}Re-MAG3-HBP) (Figure 1). In this study, ^{186}Re-MAG3-HBP was synthesized and its stability and biodistribution were studied in comparison to ^{186}Re-HEDP.

MATERIALS AND METHODS

General. Proton nuclear magnetic resonance (^{1}H NMR) spectra were recorded on a Bruker AC-200 spectrometer (JEOL Ltd., Tokyo, Japan), and the chemical shifts were reported in ppm downfield from an internal tetramethylsilane standard. Fast atom bombardment mass spectra (FAB-MS) were obtained with a JMS–HX/HX 110 A (JEOL Ltd.). Ionspray mass spectra (IS-MS) were obtained with an API*IIIE* (Parkin-Elmer Sciex Instruments, Toronto, Canada). Electrospray ionization mass spectra (ESI-MS) were obtained with a LCMS-QP8000α (Shimadzu, Kyoto, Japan). ^{186}Re was supplied by the Japan Atomic Energy Research Institute (Tokai-mura, Japan) as perrhenate ($^{186}ReO_4^-$) (*12*). Cellulose acetate electrophoresis (CAE, Separax-SP; Joko Co. Ltd., Tokyo, Japan) was run in an electrostatic field of 0.8 mA/cm for 20 min in veronal buffer (I = 0.06, pH 8.6). TLC analyses were performed with silica plates (Merck Art 5553) using acetone as a developing solvent. Benzoylmercaptoacetylglycylglycylglycine (Bz-MAG3) was supplied by Daiich Radioisotopes Labs (Chiba, Japan). Other reagents were of reagent grade and used as received.

Synthesis of ^{186}Re-MAG3-HBP. ^{186}Re-MAG3-HBP (**10**) was synthesized according to the procedure outlined in Scheme 1.

Tritylmercaptoacetic Acid (3). Mercaptoacetic acid (8.3 g, 90 mmol) and trityl chloride (25.0 g, 90 mmol) were dissolved in 45 mL of dimethylformamide (DMF). After the reaction mixture had been stirred at room temperature for 48 h, the solvent was removed in vacuo. The residue was dissolved in 100 mL of chloroform, and then 6 N NaOH was gradually added to the solution. The precipitated white crystals were collected and washed with distilled water to obtain compound **3** (22.3 g, 74.3%). ^{1}H NMR ($CDCl_3$): δ 7.43–7.19 (overlapped m, 15H), 3.03 (s, 2H). FAB-MS calcd for $C_{21}H_{18}O_2S$ $(M - H)^-$: *m/z* 333. Found: 333.

***N*-[(Tritylmercapto)acetyl]glycylglycylglycine (Tr-MAG3) (5).** Compound **3** (10.0 g, 30 mmol) was dissolved in 150 mL of chloroform, and *N*-hydroxysuccinimide (NHS) (3.45 g, 30 mmol) was added to the solution. Dicyclohexylcarbodiimide (DCC) (7.40 g, 36 mmol) in 25 mL of chloroform was added dropwise to the reaction mixture at room temperature. The reaction solution was stirred at room temperature for 18 h. The solvent was removed in vacuo. The residue was suspended in ethyl acetate. After filtration, the filtrate was evaporated in vacuo, and the residue was washed with hexane to obtain compound **4** (3.64 g) as the crude product. Glycylglycylglycine (0.73 g, 3.87 mmol) was dissolved in 22 mL of distilled water, and the solution was adjusted to pH 8.8 with 1 N NaOH. Compound **4** (2.00 g) was dissolved in 20 mL of DMF and was added dropwise to the glycylglycylglycine aqueous solution. After 3 h of stirring at 40 °C, the solvent was removed in vacuo. The residue was suspended in 30 mL of dilute hydrochloric acid (pH 2–3), and the aqueous mixture was extracted with chloroform. The organic layer was dried over anhydrous $CaSO_4$, and the solvent was removed in vacuo. The residue was purified by chromatography on silica gel using chloroform–methanol–acetic acid (50:10:1) as the eluent to obtain compound **5** (501 mg, 21.3%) as white crystals. ^{1}H NMR ($CDCl_3$): δ 7.23–7.44 (overlapped m, 15H), 4.13 (s, 4H), 3.65 (s, 2H), 3.47 (s, 2H). FAB-MS calcd for $C_{27}H_{27}N_3O_5S$ $(M + H)^+$: *m/z* 506. Found: 506.

4-Amino-1-hydroxybutylidene-1,1-bisphosphonate (7). Compound **7** was synthesized according to the procedure of Kiecykowski (*13*). Briefly, phthalic anhydride (29.6 g, 0.2 mol) was reacted with 4-aminobutyric acid (20.6 g, 0.2 mol) in 50 mL of acetic acid at 120 °C for 2 h. The reaction solution was cooled, and 300 mL of distilled water was gradually added to the solution. The precipitated white crystals were collected and washed with distilled water to obtain 4-phthalimidobutyric acid (40.5 g, 86.9%). ^{1}H NMR ($CDCl_3$): δ 7.82–7.89 (overlapped m, 2H), 7.76–7.65 (overlapped m, 2H), 3.77 (t, 2H), 2.43 (t, 2H), 2.02 (quin, 2H). FAB-MS calcd for $C_{12}H_{11}NO_4$ $(M + H)^+$: *m/z* 234. Found: 234.

4-Phthalimidobutyric acid (11.7 g, 50 mmol) was reacted with thionyl chloride (7.37 g, 62 mmol) in 50 mL of toluene and 50 μL of DMF at 50 °C for 1 h. The excess thionyl chloride was removed by distillation. The volume of the reaction mixture was reduced to 25 mL by distillation under a house vacuum (100 mmHg) at 80 °C. An additional 50 mL of toluene was added, and the mixture was distilled. The clear, colorless solution was used in the next reaction without further purification. Trimethyl phosphate (6.50 g, 53 mmol) was added, and the reaction solution was stirred at room temperature for 18 h. The reaction solution was used in the next reaction without further purification. Dimethyl phosphite (5.80 g, 53 mmol) was added to the reaction solution. Triethylamine (5.00 g, 50 mmol) was then added dropwise at 20 °C. During the addition of triethylamine, there was a rapid crystallization. After stirring for an additional 1 h, the reaction mixture was allowed to stand at 4 °C for 1 h. The precipitated white crystals were collected and washed with toluene to obtain tetramethyl 4-phthalimido-1-hydroxybutylidene-1,1-bisphosphonate

Scheme 1. Synthesis of ^{186}Re-MAG3-HBP[a]

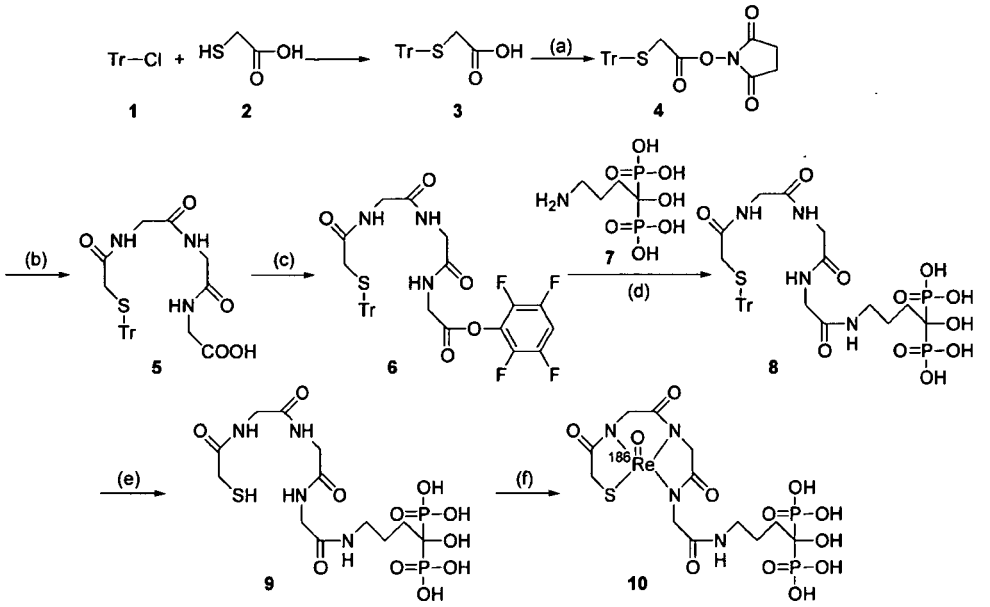

[a] Reagents: (a) NHS, DCC; (b) glycylglycylglycine; (c) TFP, DCC; (d) Et_3N; (e) TFA, triethylsilane; (f) $^{186}ReO_4^-$, $SnCl_2$/citrate.

(10.2 g, 46.9%). ^{1}H NMR ($CDCl_3$): δ 7.81–7.86 (overlapped m, 2H), 7.70–7.75 (overlapped m, 2H), 3.81–3.89 (overlapped m, 12H), 3.72 (t,2H), 2.00–2.14 (overlapped m, 4H). FAB-MS calcd for $C_{16}H_{23}NO_9P_2$ (M + H)$^+$: *m/z* 436. Found: 436.

Tetramethyl 4-phthalimido-1-hydroxybutyliden-1, 1-bisphosphonate (1.00 g, 2.3 mmol) was hydrolyzed by the reflux in 5 mL of 6 N HCl for 18 h. The resulting suspension was cooled to 0 °C, and the phthalic acid was removed by filtration. The filtrate was concentrated. Compound **7** was crystallized by the addition of 1.25 mL of water and 1.88 mL of ethanol. After the suspension was cooled at 4 °C for 2 h, compound **7** (430 mg, 75.1%) was obtained by filtration and washing with 95% ethanol as white crystals. ^{1}H NMR (NaOD/D_2O): δ 2.88 (m, 2H), 1.85 (m, 4H). FAB-MS calcd for $C_4H_{13}NO_7P_2$ (M + Na)$^+$: *m/z* 272. Found: 272.

[1-Hydroxy-1-phosphono-4-[2-[2-[2-(2-tritylmercaptoacetylamino)acetylamino]acetylamino]acetylamino]butyl]phosphonic Acid (8) (Tr-MAG3-HBP). Tr-MAG3 (**5**) (100 mg, 0.198 mmol) and tetrafluorophenol (TFP) (38.8 mg, 0.220 mmol) were dissolved in 14 mL of chloroform. DCC (45.8 mg, 0.220 mmol) in 6 mL of chloroform was added dropwise to the reaction mixture at room temperature. After 1 h of stirring at room temperature, the solvent was removed in vacuo. The residue was then suspended in an adequate volume of ethyl acetate, DCC urea was removed by filtration, and the filtrate was evaporated in vacuo to obtain crude compound **6**. Compound **6** was used in the next reaction without further purification. Compound **7** (57.0 mg, 0.229 mmol) was suspended in 3 mL of distilled water, and triethylamine (139 mg, 1.37 mmol) was added to the suspension. After a few seconds of stirring at room temperature, the suspension became clear. Compound **6** was dissolved in 4 mL of acetonitrile and then added to the reaction mixture. Triethylamine (23.1 mg, 0.229 mmol) was then added, and the reaction mixture was stirred for 3 h at room temperature. This mixture was purified by reversed phase (RP)-HPLC performed with a Cosmosil 5C_{18}-AR 300 column (10 × 150 mm; Nacalai Tesque, Kyoto, Japan) at a flow rate of 4.7 mL/min with a gradient mobile phase of 25% acetonitrile in water with 0.1% trifluoroacetic acid (TFA) to 40% acetonitrile in water with 0.1% TFA for 30 min. Chromatograms were obtained by monitoring the UV adsorption at a wavelength of 254 nm. The fraction containing compound **8** was determined by mass spectrometry and collected. The solvent was removed by lyophilization to provide compound **8** (50.3 mg, 34.5%) as white crystals. ^{1}H NMR (DMSO-d_6): δ 8.22 (t,1H), 8.18 (t, 1H), 8.10 (t, 1H), 7.81 (t, 1H), 7.25–7.36 (overlapped m, 15H), 3.63–3.76 (overlapped m, 6H), 2.98 (q, 2H), 2.85 (s, 2H), 1.67–1.85 (overlapped m, 4H). IS-MS calcd for $C_{31}H_{38}N_4O_{11}P_2S$ (M + H)$^+$: *m/z* 737. Found: 737.

[[[[(4-Hydroxy-4,4-diphosphonobutyl)carbamoylmethyl]carbamoylmethyl]carbamoylmethyl]carbamoylmethanethiolate]oxorhenium(V) (10) (^{186}Re-MAG3-HBP). The trityl group of Tr-MAG3-HBP was deprotected just before radiolabeling. Tr-MAG3-HBP (0.1 mg) was dissolved in 190 μL of TFA and 10 μL of triethylsilane and gently shaken. After removal of the solvent under a stream of N_2, 0.1 mL of 0.2 M acetate buffer (pH 3.0) was added to the residue. Stannous chloride (0.3 mg) in 0.1 mL of 0.1 M citrate-buffer (pH 5.0), and 0.1 mL of $^{186}ReO_4^-$ solution, were added to the MAG3-HBP ligand solution. The reaction mixture was vigorously stirred and allowed to react at 90 °C for 1 h. After the reaction mixture had cooled to room temperature, ^{186}Re-MAG3-HBP (**10**) was purified by RP-HPLC performed with a Cosmosil 5C_{18}-AR-300 column (4.6 × 150 mm) at a flow rate of 1 mL/min with a mixture of 0.2 M phosphate buffer (pH 6.0) and ethanol (90:10) containing 10 mM tetrabutylammoniumhydroxide.

Synthesis of Nonradioactive Re-MAG3-HBP. Nonradioactive Re-MAG3-HBP (**14**) was synthesized according to the procedure outlined in Scheme 2.

[Mercaptoacetylglycylglycylglycine]oxorhenium-(V) (12) (Re-MAG3). A procedure reported previously was employed with slight modification (*14*). Bz-MAG3 (**11**) (300 mg, 817 μmol) was dissolved in 50 mL of acetonitrile–water (6:4). Stannous chloride (616 mg, 2.73 mmol) in 50 mL of 0.1 M citrate buffer (pH 5.0) and $KReO_4$ (228 mg, 789 μmol) in 50 mL of water were added to the Bz-MAG3 solution. The reaction mixture was stirred and refluxed for 1 h. After the reaction mixture

Scheme 2. Synthesis of Re-MAG3-HBP[a]

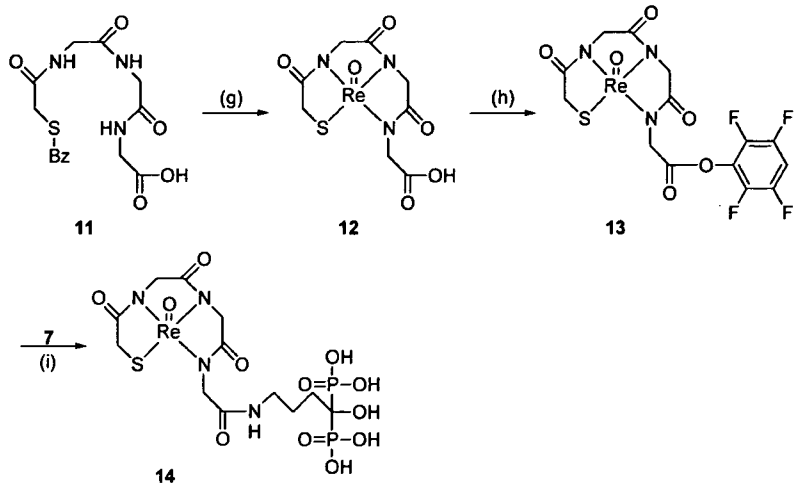

[a] Reagents: (g) $KReO_4$, $SnCl_2$/citrate; (h) TFP, DCC; (i) Et_3N.

had cooled to room temperature, Re-MAG3 was purified by RP-HPLC performed with a Cosmosil 5C_{18}-AR300 column (20 × 150 mm) at a flow rate of 12 mL/min with a gradient mobile phase of 5% acetonitrile in water with 0.1% TFA to 30% acetonitrile in water with 0.1% TFA for 30 min. Chromatograms were obtained by monitoring the UV adsorption at a wavelength of 254 nm. The fraction containing compound **12** was determined by mass spectrometry and collected. The solvent was removed by lyophilization to provide Re-MAG3 (**12**) (70.8 mg, 18.7%) as purple crystals. ESI-MS calcd for $C_8H_9N_3O_6{}^{187}ReS$ $(M - H)^-$: *m/z* 461. Found: 461, $C_8H_9N_3O_6{}^{185}ReS$ $(M - H)^-$: *m/z* 459. Found: 459.

[[[[(4-Hydroxy-4,4-diphosphonobutyl)carbamoylmethyl]carbamoylmethyl]carbamoylmethyl]carbamoylmethanethiolate]oxorhenium(V) (14) (Re-MAG3-HBP). To synthesize compound **13**, a procedure reported previously was employed with slight modifications (*15*, *16*). After Re-MAG3 (**12**) (10.0 mg, 21.6 μmol) was dissolved in 1 mL of acetate buffer (0.1 M, pH 6.0), TFP (4.15 mg, 25.0 μmol) in 100 μL of acetonitrile was added to the solution. HCl salt of 1-ethyl-3-(3-dimethylaminopropyl)carbodiimide (48.5 mg, 25.1 μmol) and triethylamine (35.0 μL, 25.2 μmol) was added to the reaction mixture. After the pH was adjusted to about 6.0 with 1 N HCl, the mixture was stirred for 30 min at room temperature. The reaction mixture was diluted with water to a volume of 8 mL and purified on two conditioned Sep-Pak C18 cartridges (Waters, Milford, MA). For washing, 20 mL of water for injection, 30 mL of 20% ethanol in 0.01 M phosphate buffer (pH 7.0), 10 mL of water and 0.5 mL of ether were used. The active ester (**13**) was eluted with 2.5 mL of acetonitrile. Compound **7** (5.38 mg, 21.6 μmol) in 1 mL of 0.1 M borate buffer (pH 9.5), and triethylamine (15.0 μL), were added to the active ester solution. After the pH was adjusted to 9.0 with 1 N NaOH, the reaction mixture was stirred for 3 h at room temperature. This reaction mixture was purified by RP-HPLC performed with a Hydrosphere C18 column (20 × 150 mm, YMC, Kyoto, Japan) at a flow rate of 14 mL/min with a gradient mobile phase of 20% acetonitrile in water with 1% formic acid to 50% acetonitrile in water with 1% formic acid for 30 min. Chromatograms were obtained by monitoring the UV adsorption at a wavelength of 254 nm. The fraction containing compound **14** was determined by mass spectrometry and collected. The solvent was removed by lyophilization to provide Re-MAG3-HBP (**14**) (1.86 mg, 12.4%) as light purple crystals. ESI-MS calcd for $C_{12}H_{20}N_4O_{12}P_2{}^{187}ReS$ $(M - H)^-$: *m/z* 692. Found: 692 $C_{12}H_{20}N_4O_{12}P_2{}^{185}ReS$ $(M - H)^-$: *m/z* 690. Found: 690.

Preparation of ^{186}Re-HEDP. ^{186}Re-HEDP was prepared according to a published procedure (*9*) and used after confirmation of its radiochemical purity by TLC ($R_f = 0$) and CAE (3.5 cm anode from the origin).

In Vitro Stability. To evaluate the stability of ^{186}Re complexes in buffered solution, ^{186}Re-labeled compounds were diluted with 0.1 M phosphate buffer (pH 7.0) saturated with 95% O_2/5% CO_2, and the solutions were incubated at 37 °C. After 1, 3, and 24 h of incubation, the samples were drawn and the radioactivity was analyzed by RP-HPLC or TLC.

Biodistribution. After HPLC purification of ^{186}Re-MAG3-HBP, solvent exchange was performed using Sep-pak C18 cartridges eluted with ethanol. The ethanol was evaporated with a stream of N_2 gas, and the residue was dissolved in saline.

Biodistribution experiments were performed by intravenously administering ^{186}Re-labeled compounds into 6-week-old male ddY mice (27−30 g). Groups of five mice were administered 100 μL of each ^{186}Re-labeled compound prior to sacrifice at 10 and 30 min, and 1, 3, 6, and 24 h postinjection. Tissues of interest were removed and weighed, and radioactivity counts were determined with an auto well gamma counter (ARC-2000; Aloka, Tokyo, Japan).

Statistical Evaluation. Biodistribution data were compared using Students' *t* test; $p = 0.05$ was defined as the limit of significance.

RESULTS

^{186}Re-MAG3-HBP (**10**) was prepared according to the method shown in Scheme 1. The precursor (Tr-MAG3-HBP (**8**)) of ^{186}Re-MAG3-HBP was synthesized by coupling the carboxyl group of Tr-MAG3 (**5**) with the amino group of a bisphosphonate derivative (**7**). The trityl group of Tr-MAG3-HBP was deprotected by treatment with TFA and triethylsilane just before radiolabeling, and ^{186}Re-MAG3-HBP (**10**) was prepared by complexation with ^{186}Re using citrate/$SnCl_2$ as a reducing system. The radiochemical yield of ^{186}Re-MAG3-HBP was 76%. After purification by RP-HPLC, ^{186}Re-MAG3-HBP showed a radiochemical purity of over 95%.

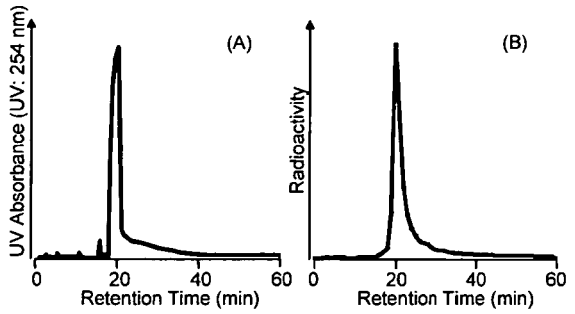

Figure 2. RP–HPLC chromatograms of (A) Re-MAG3-HBP and (B) ^{186}Re-MAG3-HBP after purification. Conditions: A flow rate of 1 mL/min with 10% ethanol in 200 mM phosphate buffer pH 6.0 containing 10 mM tetrabutylammoniumhydroxide.

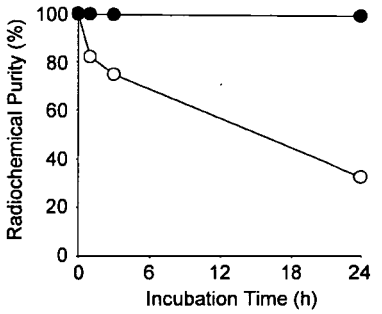

Figure 3. Stability of ^{186}Re-MAG3-HBP (closed circles) and ^{186}Re-HEDP (open circles) in buffered-solution.

Nonradioactive Re-MAG3-HBP (**14**) was synthesized by the coupling of Re-MAG3 (**12**) complexed previously with the bisphosphonate derivative (**7**), to exclude the possibility of complexation between rhenium or tin and the bisphosphonate structure (Scheme 2). Each RP-HPLC analysis of ^{186}Re-MAG3-HBP and Re-MAG3-HBP showed the same retention time (Figure 2). This indicates that the radiolabeled product proved identical to an authentic nonradioactive counterpart, and that ^{186}Re was chelated only with the MAG3 site.

Figure 3 shows the stability of ^{186}Re-MAG3-HBP and ^{186}Re-HEDP in buffered solution. After 24 h of incubation, about 95% of ^{186}Re-MAG3-HBP remained intact, whereas about 30% was intact in the case of ^{186}Re-HEDP.

The biodistributions of ^{186}Re-MAG3-HBP and ^{186}Re-HEDP in normal mice are presented in Tables 1 and 2, respectively. ^{186}Re-MAG3-HBP showed a rapid accumulation and long residence in the bone, and its uptake by the bone was significantly higher than that of ^{186}Re-HEDP. Furthermore, ^{186}Re-MAG3-HBP showed a faster clearance from the blood than did ^{186}Re-HEDP. Therefore, ^{186}Re-MAG3-HBP showed significantly higher bone:blood ratios of radioactivity than ^{186}Re-HEDP (Figure 4). Meanwhile, ^{186}Re-MAG3-HBP showed a significantly lower uptake by the stomach than ^{186}Re-HEDP.

DISCUSSION

The basic requirements of internal radiotherapeutic agents for the palliation of metastatic bone pain include excellent stability in vivo and marked accumulation in bone.

On the basis of the concept of bifunctional radiopharmaceuticals, we designed a ^{186}Re-labeled MAG3-conjugated bisphosphonate derivative (^{186}Re-MAG3-HBP, Figure 1). MAG3 was selected as the ^{186}Re-chelating group because it could form a stable, compact, and hydrophilic complex with ^{186}Re in high yield (*15*, *16*).

Table 1. Biodistribution of Radioactivity after Intravenous Administration of ^{186}Re-MAG3-HBP in Mice[a]

tissue	10 min[b]	30 min[b]	1 h[b]	3 h[b]	6 h[b]	24 h[b]
blood	3.05	0.68[d]	0.15[d]	0.05[d]	0.04[d]	0.01[d]
	(0.32)	(0.16)	(0.03)	(0.01)	(0.01)	(0.00)
liver	0.91[d]	0.40[d]	0.30[d]	0.22[d]	0.25[d]	0.12[d]
	(0.09)	(0.15)	(0.07)	(0.06)	(0.06)	(0.01)
kidney	5.40	4.35	2.42	1.30[d]	1.32	0.56
	(1.05)	(2.30)	(0.84)	(0.13)	(0.28)	(0.07)
intestine	0.70	0.44[d]	0.51[d]	0.59[d]	0.73	0.09
	(0.12)	(0.05)	(0.14)	(0.15)	(0.19)	(0.03)
spleen	0.74	0.26	0.14[d]	0.10[d]	0.10	0.08
	(0.23)	(0.09)	(0.07)	(0.02)	(0.05)	(0.02)
pancreas	0.77	0.23	0.12[d]	0.07[d]	0.08	0.05[d]
	(0.07)	(0.03)	(0.05)	(0.04)	(0.05)	(0.02)
lung	2.20	0.66	0.26[d]	0.21	0.20	0.08
	(0.51)	(0.18)	(0.06)	(0.06)	(0.03)	(0.03)
stomach[c]	0.46[d]	0.38[d]	0.25[d]	0.23[d]	0.21[d]	0.14
	(0.22)	(0.11)	(0.07)	(0.10)	(0.11)	(0.08)
femur	18.51[d]	27.19[d]	26.65[d]	28.78[d]	27.65[d]	24.51[d]
	(2.02)	(4.40)	(2.91)	(3.41)	(2.04)	(2.83)
muscle	0.84	0.23	0.45	0.09	0.06	0.18
	(0.55)	(0.14)	(0.37)	(0.06)	(0.04)	(0.16)

[a] Expressed as % injected dose per gram. Each value represents the mean (SD) for five animals at each interval. [b] Time after administration. [c] Expressed as % injected dose. [d] Significant difference.

Table 2. Biodistribution of Radioactivity after Intravenous Administration of ^{186}Re-HEDP in Mice[a]

tissue	10 min[b]	30 min[b]	1 h[b]	3 h[b]	6 h[b]	24 h[b]
blood	2.82	1.28	0.78	0.36	0.24	0.04
	(0.38)	(0.26)	(0.11)	(0.04)	(0.03)	(0.02)
liver	1.19	0.81	0.75	0.51	0.42	0.08
	(0.24)	(0.11)	(0.11)	(0.09)	(0.06)	(0.01)
kidney	6.38	6.78	5.40	1.60	1.27	0.36
	(1.50)	(5.49)	(3.79)	(0.24)	(0.04)	(0.13)
intestine	0.62	0.71	0.88	0.86	0.96	0.15
	(0.10)	(0.20)	(0.14)	(0.17)	(0.15)	(0.08)
spleen	0.70	0.31	0.25	0.15	0.09	0.06
	(0.15)	(0.05)	(0.05)	(0.02)	(0.01)	(0.04)
pancreas	1.02	0.28	0.21	0.13	0.07	0.02
	(0.38)	(0.04)	(0.02)	(0.03)	(0.02)	(0.02)
lung	1.90	0.72	0.60	0.27	0.19	0.06
	(0.36)	(0.16)	(0.19)	(0.04)	(0.03)	(0.02)
stomach[c]	0.98	1.31	1.70	1.38	0.70	0.39
	(0.10)	(0.35)	(0.37)	(0.15)	(0.19)	(0.42)
femur	12.71	14.67	17.47	13.60	14.87	11.78
	(2.05)	(1.82)	(2.82)	(2.26)	(1.29)	(3.67)
muscle	0.88	0.41	0.20	0.07	0.04	0.04
	(0.36)	(0.29)	(0.15)	(0.07)	(0.04)	(0.04)

[a] Expressed as % injected dose per gram. Each value represents the mean (SD) for five animals at each interval. [b] Time after administration. [c] Expressed as % injected dose.

The result of in vitro stability experiments indicates that ^{186}Re-MAG3-HBP is more stable than ^{186}Re-HEDP. This result was reflected in the biodistribution. Namely, since accumulation in the stomach is an index of the decomposition of a Re-complex in biodistribution studies (*17*, *18*), a low level of ^{186}Re-MAG3-HBP in the stomach indicates good stability in vivo. The blood clearance could be also influenced by this stability. When calculated from the results of the biodistribution experiments, the rate of blood clearance of ^{186}Re-MAG3-HBP and ^{186}Re-HEDP was 49.7 mL/h and 15.6 mL/h, respectively. ^{186}Re-HEDP complex gave rise to $^{186}ReO_4^-$ in vivo, and the clearance from blood of $^{186}ReO_4^-$ was slower than that of ^{186}Re-HEDP (*9*). It is suggested that the more rapid clearance from the blood of ^{186}Re-MAG3-HBP is responsible for its stability, when compared with ^{186}Re-HEDP. This rapid clearance could lead to a decrease in the level of unnecessary radiation.

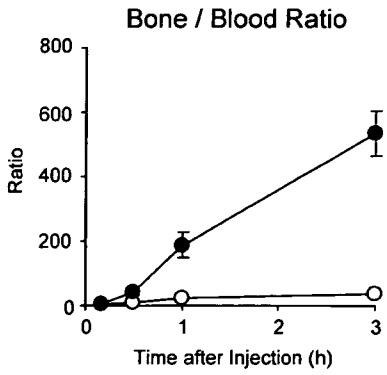

Figure 4. Bone blood ratios of radioactivity after injection of ^{186}Re-MAG3-HBP (closed circles) and ^{186}Re-HEDP (open circles) in mice.

The bone uptake of ^{186}Re-MAG3-HBP was compared with ^{186}Re-HEDP in mice. When expressed as %dose/g tissue × body weight in order to correct the difference in weight of the animals (*19*, *20*), the uptake of ^{186}Re-MAG3-HBP and ^{186}Re-HEDP in the femur 24 h after injection was 711% and 342%, respectively, while the uptake of ^{186}Re-MAG3-HBP was more than twice that of ^{186}Re-HEDP. Furthermore, bone uptake of ^{186}Re-MAG3-HBP was almost the same as that of ^{131}I-labeled arylalkylidenebisphosphonate reported recently (850%) (*19*). This ^{131}I-labeled bisphosphonate analogue was designed based on the same concept as ^{186}Re-MAG3-HBP, i.e., both compounds have a stable labeling site distinct from the bisphosphonate frame. Thus, the results obtained with the ^{131}I-labeled bisphosphonate support the usefulness of the drug design of ^{186}Re-MAG3-HBP based on bifunctional radiopharmaceuticals. In addition, $^{89}SrCl_2$ and ^{153}Sm-EDTMP were approved by the Food and Drug Administration for the treatment of painful osseous metastases, and the uptake value was 354% ($^{89}SrCl_2$, 24 h, mice) (*21*) and 580% (^{153}Sm-EDTMP, 24 h, rats) (*22*), respectively. Since the value of ^{186}Re-MAG3-HBP is higher than each of the values of $^{89}SrCl_2$ and ^{153}Sm-EDTMP, it is expected that ^{186}Re-MAG3-HBP will be of clinical use.

In conclusion, we developed a highly stable ^{186}Re-labeled bisphosphonate, ^{186}Re-MAG3-HBP. This agent showed a marked accumulation in bone and rapid clearance from other tissues. Thus, ^{186}Re-MAG3-HBP is expected to be a useful radiopharmaceutical for the palliation of metastatic bone pain.

ACKNOWLEDGMENT

This work was supported in part by Grants-in-Aid for Young Scientists (13770500 and 15790665) and Exploratory Research (13877381) from the Ministry of Education, Culture, Sports, Science and Technology of Japan.

LITERATURE CITED

(1) Yoneda, T., Sasaki, A., and Mundy, G. R. (1994) Osteolytic bone metastasis in breast cancer. *Breast Cancer Res. Treat. 32*, 73–84.

(2) Arcangeli, G., Giovinazzo, G., Saracino, B., D'Angelo, L., Giannarelli, D., and Micheli, A. (1998) Radiation therapy in the management of symptomatic bone metastases: the effect of total dose and histology on pain relief and response duration. *Int. J. Radiat. Oncol. Biol. Phys. 42*, 1119–1126.

(3) Silberstein, E. B., and Williams, C. (1985) Strontium-89 therapy for the pain of osseous metastases. *J. Nucl. Med. 26*, 345–348.

(4) Robinson, R. G., Preston, D. F., Schiefelbein, M., and Baxter, K. G. (1995) Strontium 89 therapy for the palliation of pain due to osseous metastases. *JAMA 274*, 420–424.

(5) Elder, R. C., Yuan, J., Helmer, B., Pipes, D., Deutsch, K., and Deutsch, E. (1997) Studies of the structure and composition of rhenium-1,1-hydroxyethylidenediphosphonate (HEDP) analogues of the radiotherapeutic agent ^{186}ReHEDP. *Inorg. Chem. 36*, 3055–3063.

(6) Kolesnikov-Gauthier, H., Carpentier, P., Depreux, P., Vennin, P., Caty, A., and Sulman, C. (2000) Evaluation of toxicity and efficacy of ^{186}Re-hydroxyethylidene diphosphonate in patients with painful bone metastases of prostate or breast cancer. *J. Nucl. Med. 41*, 1689–1694.

(7) Limouris, G. S., Shukla, S. K., Condi-Paphiti, A., Gennatas, C., Kouvaris, I., Vitoratos, N., Manetou, A., Dardoufas, C., Rigas, V., and Vlahos, L. (1997) Palliative therapy using rhenium-186-HEDP in painful breast osseous metastases. *Anticancer Res. 17*, 1767–1772.

(8) de Klerk, J. M., van Dijk, A., van het Schip, A. D., Zonnenberg, B. A., and van Rijk, P. P. (1992) Pharmacokinetics of rhenium-186 after administration of rhenium-186-HEDP to patients with bone metastases. *J. Nucl. Med. 33*, 646–651.

(9) Arano, Y., Ono, M., Wakisaka, K., Uezono, T., Akizawa, H., Motonari, Y., Makata, Y., Konishi, J., and Yokoyama, A. (1995) Synthesis and biodistribution studies of ^{186}Re complex of 1-hydroxyethylidene-1,1-diphosphonate for treatment of painful osseous metastases. *Radioisotopes 44*, 514–522.

(10) De Winter, F., Brans, B., Van De Wiele, C., and Dierckx, R. A. (1999) Visualization of the stomach on rhenium-186 HEDP imaging after therapy for metastasized prostate carcinoma. *Clin. Nucl. Med. 24*, 898–899.

(11) Rogers, M. J., Watts, D. J., and Russell, R. G. (1997) Overview of bisphosphonates. *Cancer 80*, 1652–1660.

(12) Kobayashi, K., Motoishi, S., Terunuma, K., Rauf, A. A., and Hashimoto, K. (2000) Production of $^{186/188}$Re and recovery of tungsten from spent ^{188}W/^{188}Re generator. *Radiochemistry 42*, 551–554.

(13) Kieczykowski, G. R. (1992) New process for preparing an antihypercalcemic agent. UK Patent GB 2248061A.

(14) Guhlke, S., Schaffland, A., Zamora, P. O., Sartor, J., Diekmann, D., Bender, H., Knapp, F. F., and Biersack, H. J. (1998) ^{188}Re- and ^{99m}Tc-MAG3 as prosthetic groups for labeling amines and peptides: approaches with pre- and postconjugate labeling. *Nucl. Med. Biol. 25*, 621–631.

(15) Visser, G. W., Gerretsen, M., Herscheid, J. D., Snow, G. B., and van Dongen, G. (1993) Labeling of monoclonal antibodies with rhenium-186 using the MAG3 chelate for radioimmunotherapy of cancer: a technical protocol. *J. Nucl. Med. 34*, 1953–1963.

(16) van Gog, F. B., Visser, G. W., Klok, R., van der Schors, R., Snow, G. B., and van Dongen, G. A. (1996) Monoclonal antibodies labeled with rhenium-186 using the MAG3 chelate: relationship between the number of chelated groups and biodistribution characteristics. *J. Nucl. Med. 37*, 352–362.

(17) Lin, W. Y., Hsieh, J. F., Tsai, S. C., Yen, T. C., Wang, S. J., and Knapp, F. F., Jr. (2000) A comprehensive study on the blockage of thyroid and gastric uptakes of ^{188}Re-perrhenate in endovascular irradiation using liquid-filled balloon to prevent restenosis. *Nucl. Med. Biol. 27*, 83–87.

(18) Deutsch, E., Libson, K., Vanderheyden, J. L., Ketring, A. R., and Maxon, H. R. (1986) The chemistry of rhenium and technetium as related to the use of isotopes of these elements in therapeutic and diagnostic nuclear medicine. *Nucl. Med. Biol. 13*, 465–477.

(19) Årstad, E., Hoff, P., Skattebøl, L., Skretting, A., and Breistøl, K. (2003) Studies on the synthesis and biological properties of noncarrier-added [^{125}I and ^{131}I]-labeled arylalkylidenebisphosphonates: potent bone-seekers for diagnosis and therapy of malignant osseous lesions. *J. Med. Chem. 46*, 3021–3032.

(20) Larsen, R. H., Murud, K. M., Akabani, G., Hoff, P., Bruland, O. S., and Zalutsky, M. R. (1999) ^{211}At- and

^{131}I-labeled bisphosphonates with high in vivo stability and bone accumulation. *J. Nucl. Med. 40*, 1197−1203.

(21) Henriksen, G., Fisher, D. R., Roeske, J. C., Bruland, O. S., and Larsen, R. H. (2003) Targeting of osseous sites with alpha-emitting ^{223}Ra: comparison with the beta-emitter ^{89}Sr in mice. *J. Nucl. Med. 44*, 252−259.

(22) Laznicek, M., Laznickova, A., Budsky, F., Prokop, J., and Kopicka, K. (1994) Comparison of biological characteristics of EDTMP complexes with ^{99m}Tc, ^{111}In and ^{153}Sm in rats. *Appl. Radiat. Isot. 45*, 949−953.

BC040249W

Available online at www.sciencedirect.com
SCIENCE DIRECT
Nuclear Medicine and Biology 32 (2005) 21–28
NUCLEAR MEDICINE — AND — BIOLOGY
www.elsevier.com/locate/nucmedbio

Basic characterization of ^{64}Cu-ATSM as a radiotherapy agent

Atsushi Obata[a,b], Shingo Kasamatsu[c], Jason S. Lewis[d], Takako Furukawa[a], Shinji Takamatsu[a], Jun Toyohara[e], Tatsuya Asai[a], Michael J. Welch[d], Susan G. Adams[d], Hideo Saji[b], Yoshiharu Yonekura[a], Yasuhisa Fujibayashi[a,*]

[a]*Biomedical Imaging Research Center, University of Fukui, Matsuoka, Fukui 910-1193, Japan*
[b]*Graduate School of Pharmaceutical Sciences, Kyoto University, Sakyo, Kyoto 606-8151, Japan*
[c]*JFE Fukui Branch, University of Fukui, Matsuoka, Fukui 910-1193, Japan*
[d]*Mallinckrodt Institute of Radiology, Washington University Medical Center, St. Louis, MO 63110, USA*
[e]*Research Center, Research and Development Division, Nihon Medi-Physics, Co. Ltd., Chiba 910-1193, Japan*

Received 24 March 2004; received in revised form 29 July 2004; accepted 20 August 2004

Abstract

^{64}Cu-diacetyl-bis(N^4-methylthiosemicarbazone) (^{64}Cu-ATSM) is a promising radiotherapy agent for the treatment of hypoxic tumors. In an attempt to elucidate the radiobiological basis of ^{64}Cu-ATSM radiotherapy, we have investigated the cellular response patterns in vitro cell line models. Cells were incubated with ^{64}Cu-ATSM, and the dose–response curves were obtained by performing a clonogenic survival assay. Radiation-induced damage in DNA was evaluated using the alkali comet assay and apoptotic cells were detected using Annexin V-FITC and propidium iodide staining methods. Washout rate and subcellular distribution of ^{64}Cu in cells were investigated to further assess the effectiveness of ^{64}Cu-ATSM therapy on a molecular basis. A direct comparison of subcellular localization of Cu-ATSM was made with the flow tracer analog Cu-pyruvladehyde-bis(N^4-methylthiosemicarbazone). In this study, ^{64}Cu-ATSM was shown to reduce the clonogenic survival rate of tumor cells in a dose-dependent manner. Under hypoxic conditions, cells took up ^{64}Cu-ATSM and radioactive ^{64}Cu was highly accumulated in the cells. In the ^{64}Cu-ATSM-treated cells, DNA damage by the radiation emitted from ^{64}Cu was detected, and inhibition of cell proliferation and induction of apoptosis was observed at 24 and 36 h after the treatment. The typical features of postmitotic apoptosis induced by radiation were observed following ^{64}Cu-ATSM treatment. The majority of the ^{64}Cu taken up into the cells remained in the postmitochondrial supernatant (the cellular residue after removal of the nuclei and mitochondria), which indicates that the β^- particle emitted from ^{64}Cu may be as effective as the Auger electrons in ^{64}Cu-ATSM therapy. These data allow us to postulate that ^{64}Cu-ATSM will be able to attack the hypoxic tumor cells directly, as well as potentially affecting the peripheral nonhypoxic regions indirectly by the β^- particle decay of ^{64}Cu.

Keywords: ^{64}Cu-ATSM; Tumor; Internal radiation therapy; Hypoxia; Apoptosis; PET

1. Introduction

Radionuclide therapy is one of the highly promising approaches for treating cancer and is widely investigated in basic research and clinical practice [1]. Radionuclide therapies using labeled antibodies or peptides targeting tumor-related antigens or receptors have been extensively studied especially in the field of hematological malignancies such as lymphoma and leukemia [2–4]. However, success of these agents in solid tumors has been limited mainly due to heterogeneous antigen expression and low overall tumor uptake. A variety of strategies have been employed to improve the tumor targeting and therapy effects of such methods including combination therapy with other modalities [5–8].

Conventionally, low linear energy transfer β-emitters such as ^{131}I, ^{90}Y and ^{186}Re have been widely used for radionuclide therapy [9]. ^{67}Cu also has been investigated as a candidate for radionuclide therapy. ^{67}Cu has excellent physical and biochemical properties for radionuclide therapy and ^{67}Cu-labeled monoclonal antibodies were reported to be useful for the treatment of lymphoma and colorectal carcinoma [9,10]. However, production of ^{67}Cu requires a large accelerator or nuclear reactor, limiting the availability of ^{67}Cu.

* Corresponding author. Tel.: +81 776 61 8430; fax: +81 776 61 8170.
E-mail address: yfuji@fmsrsa.fukui-med.ac.jp (Y. Fujibayashi).

0969-8051/$ – see front matter © 2005 Elsevier Inc. All rights reserved.
doi:10.1016/j.nucmedbio.2004.08.012

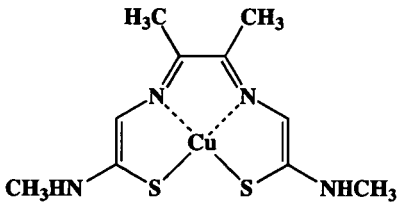

Fig. 1. Structure of Cu-ATSM.

^{64}Cu with a half-life of 12.7 h decays by electron capture (41%), β^- decay (0.573 MeV, 40%) and β^+ decay (0.656 MeV, 19%), accompanied by emission of annihilation radiation (0.511 MeV, 38%) and γ photons (1.34 MeV, 0.5%). It is a promising therapeutic radionuclide because of its favorable β^- particle emissions [11,12]. ^{64}Cu is reported to be as efficient as ^{67}Cu for tumor treatment [13,14] and can be produced using small biomedical cyclotrons in regular PET centers on a daily basis [15,16]. Furthermore, because of its multiple decay modes, ^{64}Cu can be used for real-time PET monitoring of regional drug concentration, kinetics and dosimetry during radiation therapy if it is used to label the therapeutic radiopharmaceuticals.

Copper-diacetyl-bis(N^4-methylthiosemicarbazone) (Cu-ATSM; Fig. 1) has been examined extensively by our group and others as a possible imaging agent to delineate hypoxia within tumors [12,17,18]. Cu-ATSM is taken up into tumor cells rapidly and efficiently and reduced by an enzymatic system of sequential electron transport chains, where monovalent Cu is released from the chelate to be retained subsequently [19]. Considering these characters, ^{64}Cu-ATSM has potential as a radiotherapy agent with an option of real-time PET monitoring. Indeed, as a therapy agent, ^{64}Cu-ATSM was reported to be useful for the treatment of colorectal carcinoma in vivo tumor model [20]. In the present report, we have investigated the molecular basis of ^{64}Cu-ATSM therapy using in vitro tumor cell models. The cell killing ability of ^{64}Cu-ATSM was evaluated by colony-forming assay. Some of the typical features of cell death derived by radiation were observed; namely, inhibition of the cell proliferative rate and apoptotic cell death. Subcellular localization of Cu-ATSM was studied and compared with Cu-pyruvladehyde-bis(N^4-methylthiosemicarbazone) (Cu-PTSM), a flow tracer [21]. We also discuss the fate of ^{64}Cu in relation to cell toxicity. This study may provide useful information for designing effective therapy strategies and improving the radiotherapy efficacy in cancer treatment.

2. Materials and methods

All chemicals were reagent grade. The ^{64}Cu at University of Fukui was produced on a 12-MeV biomedical cyclotron using previously reported methods [15,16]. The ^{64}Cu at Washington University was produced on a CS-15 biomedical cyclotron (Cyclotron) [15]. H_2ATSM was synthesized as described previously [22]. ^{64}Cu-ATSM was prepared by mixing 200 mM glycine buffer containing ^{64}Cu and H_2ATSM in dimethyl sulfoxide (20:1 by volume) [17]. Labeling efficiency was determined by radio-HPLC using conditions described previously [19]. Radiochemical purity and specific activity of ^{64}Cu-ATSM in all studies were >99% and >56,000 GBq/mmol, respectively.

2.1. Cell culture

Mouse Lewis Lung carcinoma LL/2 cells were purchased from Dai-Nippon Seiyaku (Japan) and were grown in a 5% CO_2-humidified atmosphere at 37 °C. Cells were routinely maintained in Dulbecco's modified Eagle Medium (DMEM) (GIBCO, Grand Island, NY) supplemented with 10% fetal bovine serum.

2.2. Uptake of ^{64}Cu-ATSM into cells

Previous reports show that the uptake of ^{64}Cu-ATSM was dramatically increased under hypoxic conditions [23]; therefore, we followed the reported methods during the uptake phase. Briefly, cells were trypsinized and collected in a polypropylene tube (Falcon, Becton Dickinson, Lincoln Park, NJ). Cell numbers were counted with a hemocytometer and the cells were resuspended in serum-free DMEM to a concentration of 1×10^6 cells/ml. Ten million cells were transferred to a three-necked flask and hypoxic gas (95% N_2, 5% CO_2) was passed over the cells at 37 °C for 1.5 h. ^{64}Cu-ATSM was then added to the flask and incubated for 1 h. After incubation, aliquots of the cell suspension were removed and the cells were pelleted from the reaction media to calculate the percentage uptake of ^{64}Cu-ATSM. Additional aliquots of cells were transferred to a polypropylene tube and resuspended with fresh DMEM containing 10% fetal bovine serum for further experiments.

2.3. Clonogenic survival assay

The radiotherapy effect of ^{64}Cu-ATSM was measured by performing a clonogenic survival assay under normoxic condition [24,25] because continuous hypoxia treatment itself affected cell viability. The ^{64}Cu-ATSM-treated cells, resuspended in fresh medium, were counted using a hemocytometer and diluted properly. Cells were seeded into 60-mm dishes (Falcon, Becton Dickinson, Lincoln Park, NJ) and cultured in a humidified 5% CO_2/95% air atmosphere at 37 °C. After 5 days of incubation, the cells were stained with 3% Giemsa solution, and colonies containing more than 50 cells were counted as survivors. The absolute plating efficiencies of control cells were 34.1±9.7%. The surviving fraction was determined as the ratio of live colonies in the ^{64}Cu-ATSM-treated cell populations relative to the glycine-treated control.

2.4. Cell growth assay

After the treatment, cells were seeded in six-well plates (Falcon, Becton Dickinson, Lincoln Park, NJ) and cultured

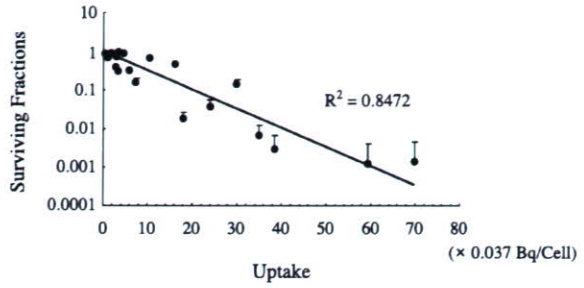

Fig. 2. Clonogenic survival of LL/2 cells treated with ^{64}Cu-ATSM. LL/2 cells were treated with different concentrations of ^{64}Cu-ATSM for 1 h under hypoxic conditions to trap ^{64}Cu metabolically into cells. After the treatment, surplus ^{64}Cu-ATSM was removed and cells were resuspended in fresh culture medium and the radioactivity taken up by the cells was measured. Cells were seeded in 6-cm dishes and cultured for 5 days, and the colonies containing more than 50 cells were counted. The surviving fractions determined as described in Materials and methods was plotted against the amount of ^{64}Cu taken up by the cells. Values are the mean and S.D. ($n=6$).

under normoxic condition. Cells were trypsinized and counted using the trypan blue dye exclusion test at the specified time points.

2.5. Comet assay (single cell gel electrophoresis)

To detect the damage to DNA induced by ^{64}Cu, the comet assay was performed after ^{64}Cu-ATSM treatment [26]. Glycine-treated control cells and ^{64}Cu-ATSM-treated cells were seeded in 100-mm dishes (Falcon, Becton Dickinson) and cultured under normoxic condition. Six hours after the treatment, cells were trypsinized and counted using the trypan blue dye exclusion test. Viability of cells was >90%. The cells were sedimented by centrifugation and adjusted to the concentration of 1×10^5 cells/ml with phosphate-buffered saline. The cells were treated with a

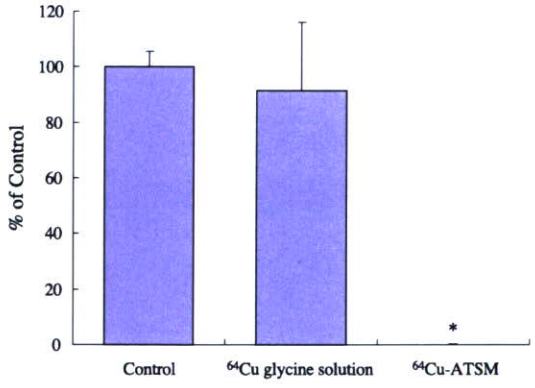

Fig. 3. The effect of carrier-free ^{64}Cu and ^{64}Cu-ATSM on the survival rate of LL/2 cells. A clonogenic survival assay was performed with a control group (treated with glycine solution), a ^{64}Cu-glycine solution-treated group (938.3±41.65 μCi added to 10^7 cells) and a ^{64}Cu-ATSM-treated group (896.7±35.84 μCi added to 10^7 cells). Viability compared with control group was 91.43±24.64% and 0.1247±0.2874%, respectively. *$P<.0001$, significant degrease compared with control (Student's t test, $n=3$).

Table 1
^{64}Cu uptake ratio and radioactivity in tumor cells after 1 h of treatment

	% Uptake	Radioactivity in tumor cells (Bq/cell)
^{64}Cu-glycine	2.47±0.46	0.0857±0.0038
^{64}Cu-ATSM	61.4±17.7	2.04±0.08

Data are expressed as the mean±S.D. ($n=3$).

CometAssay Kit (Trevigen, Gaithersvurg, MD) according to the instruction manual from the manufacturer. After electrophoresis, assay slides were treated with CometAssay Silver Staining Kit (Trevigen) to visualize the assay results. Data analysis was performed using Komet v. 4.0.2 software (Kinetic Imaging, Wirral, UK).

2.6. Measurement of apoptotic cell death

Early stages of apoptosis were identified using an Annexin V-FITC Apoptosis Detection Kit I (Becton Dickinson, San Jose, CA) [27]. After the uptake period, cells were seeded in six-well plates and cultured under normoxic condition. At the specified time points, cells were collected and stained with Annexin V-FITC/propidium iodide (PI) according to the manufacturer's protocol. Level of apoptosis was quantified using a Becton Dickinson FACSCalibur system and analyzed using CellQuest v. 3.1 software (Becton Dickinson, San Jose, CA). Cells that were Annexin

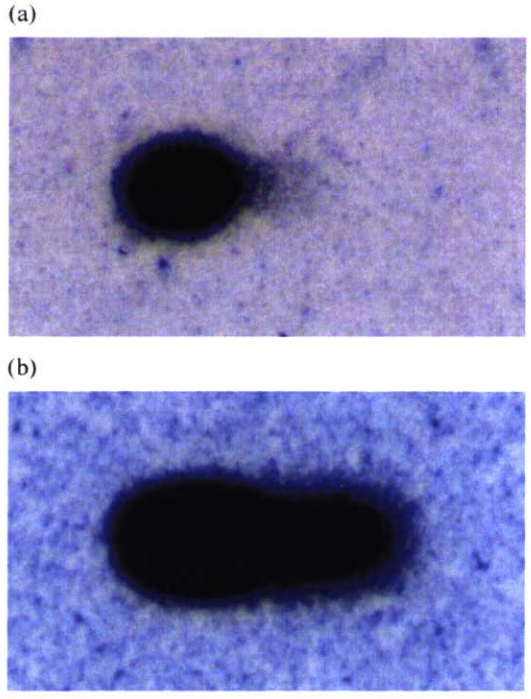

Fig. 4. The typical microscopic images following the comet assay at 6 h after treatment. Images of a normal cell (a) and DNA-damaged cell (b) are shown. In the ^{64}Cu-ATSM-treated groups, over 90% of total cells suffered from DNA damage and displayed damaged pattern as shown in b.

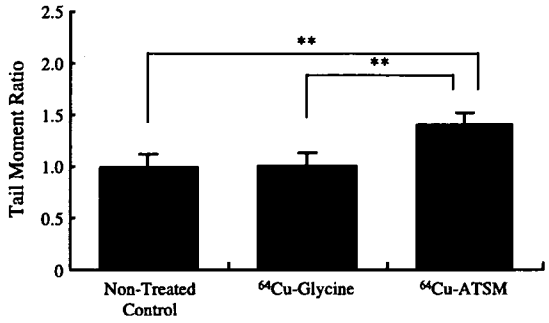

Fig. 5. Tail moment ratio in the comet assay. Forty cells were selected ad libitum and then analyzed for the tail moment using the Comet v. 4.0.2 software. Data are presented as a ratio to the nontreated control groups (bar, 1 S.E.). $**P<.01$, significant increase (Student's t test).

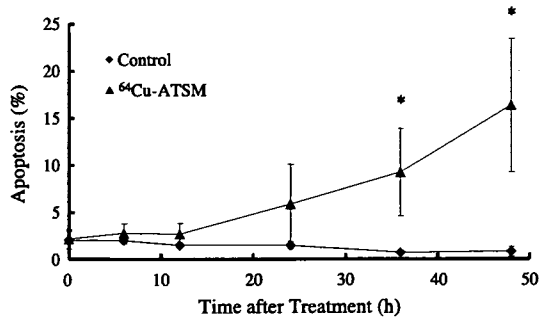

Fig. 7. Apoptosis of LL/2 cells after ^{64}Cu-ATSM treatment. Floating and adherent cells were collected, stained with Annexin V-FITC and PI, then analyzed by FACS using CellQuest software. A significant increase in apoptosis was observed with ^{64}Cu-ATSM-treated cells from 36 h after the treatment. Data points are the average percentage of apoptotic cells and S.D. ($n=3$). $*P<.05$, significant increase (Student's t test).

V-FITC-positive and PI-negative were identified as apoptotic cells as described previously [28,29].

2.7. Retention and intracellular distribution of ^{64}Cu-ATSM and ^{64}Cu-PTSM in LL/2 cells

Cells were incubated in hypoxic gas (95% N_2, 5% CO_2) for 1.5 h at which point either ^{64}Cu-ATSM or ^{64}Cu-PTSM was added to the media. Following a 1-h incubation, the media was removed and the cells in fresh medium were seeded in 100-mm dishes, cultured under normoxic condition and recollected at 0, 1, 3, 6, 12 and 24 h after the treatment. Cells were washed twice with an ice-cold isolation medium (0.25 M sucrose buffered to pH 7.4 with 10 mM HEPES). Aliquots of cells were separated and the radioactivity in the cells was counted using a γ-counter (ARC-2000, ALOKA, Japan). Another aliquot of the cells was resuspended in ice-cold lysis buffer (0.005% SDS buffered to pH 7.4 with 10 mM HEPES) and homogenized. After homogenization, the P1 fraction (crude nuclear fraction) was obtained by centrifugation at $1000\times g$ for 5 min at 4 °C. The supernatant was centrifuged at $8000\times g$ for 10 min at 4 °C to yield the P2 (crude mitochondrial) and S2 (the postmitochondrial supernatant which contains the cellular residue after removal of the nuclei and mitochondria) fraction. Radioactivity in each fraction was measured.

3. Results

Fig. 2 shows the radiation dose–response curve for the LL/2 cells treated with ^{64}Cu-ATSM. Clonogenic survival was decreased in a dose-dependent manner. ^{64}Cu-ATSM uptake of 1.50 Bq/cell produced 99% killing of the cells. Mock treatment with H_2ATSM or nonradioactive Cu-ATSM did not affect the survival ratio of LL/2 cells (data not shown), which also indicates that hypoxia treatment during uptake phase did not affect the cell viability by itself.

The effect of "free" ^{64}Cu ion and ^{64}Cu-ATSM on tumor cells was also compared using the clonogenic survival assay. When approximately 34.8 MBq of ^{64}Cu-glycine solution was inoculated, the survival rate of cells was not affected, whereas the equivalent amount of ^{64}Cu-ATSM treatment produced nearly complete killing of LL/2 cells (Fig. 3). The ^{64}Cu uptake ratio in each treatment was 2.47±0.459% and 61.4±17.7%, respectively, which means the radioactivity

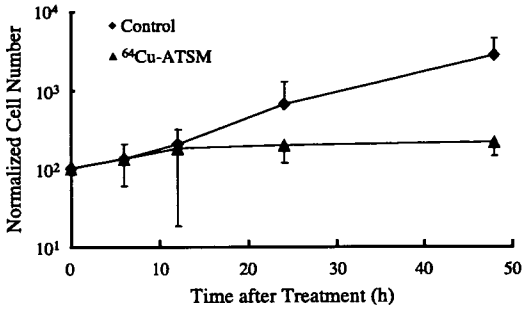

Fig. 6. Growth curve of LL/2 cells after ^{64}Cu-ATSM treatment. Proliferation of the cells was inhibited 24 h after the treatment. Data are presented as normalized cell number ± S.D. relative to time 0 ($n=3$).

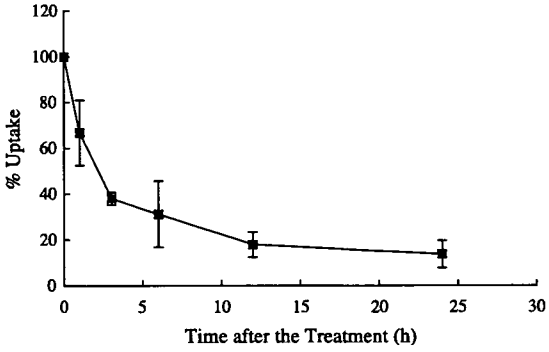

Fig. 8. Washout rate of ^{64}Cu from LL/2 cells; 1×10^7 cells were treated with ^{64}Cu-ATSM and radioactivity in the cell fractions was measured at each time point. Data are shown as ratio to the initial radioactivity after the decay correction. Each data point is the average ± S.D. ($n=3$).

taken up into tumor cells was 0.0857 ± 0.0038 and 2.04 ± 0.08 Bq/cell, respectively. The result suggests that intracellular uptake is the major factor in the efficient tumor cell killing by ^{64}Cu-ATSM (Table 1).

To elucidate the mechanism of cell killing by ^{64}Cu-ATSM, the comet assay was performed 6 h after the ^{64}Cu-ATSM treatment. Fig. 4 shows a typical microscopic image of the results. In the ^{64}Cu-ATSM-treated groups, over 90% of the total cells showed comet tails. The tail moment ratio was significantly increased in the ^{64}Cu-ATSM-treated groups compared with ^{64}Cu-glycine and nontreated control groups (Fig. 5) (nontreated group, $P=.0085$; ^{64}Cu-glycine-treated group, $P=.0085$). These results indicated that the radiation emitted from the intracellular ^{64}Cu caused DNA strand breaks, with the maximum recoil energy from the transmutation of ^{64}Cu to its highly charged daughter nucleus potentially increasing the cell killing ability. This damage in the DNA is thought to be one of the major triggers of cell death pathways. Fig. 6 shows the proliferation rate of LL/2 cells after the treatment. In the ^{64}Cu-ATSM-treated group, cell proliferation was completely inhibited after 24 h and a significant apoptotic fraction was seen 36 h after the treatment ($P<.05$) (Fig. 7).

Both the washout rate and subcellular distribution of ^{64}Cu were investigated in this study. Also, a direct comparison of the subcellular localization was made between ^{64}Cu-ATSM and ^{64}Cu-PTSM. With ^{64}Cu-ATSM, defining the amount of radioactivity associated with the cells at the time of resuspension as 100%, 38.0% of the radioactivity remained at 3 h posttreatment and 31.2% at 6 h posttreatment (Fig. 8). Considering the half-life of ^{64}Cu, the effect of radiation emitted from ^{64}Cu up to 12 h after treatment dominates in this study: about 14,200 decays occurred in one cell up to 12 h after treatment (Fig. 9). In the subcellular fractionation comparison, the distribution of ^{64}Cu from both ^{64}Cu-ATSM and ^{64}Cu-PTSM was very similar (Fig 10). For both ^{64}Cu-ATSM and ^{64}Cu-PTSM, the majority of the radioactivity remained in the S2 fraction over the 24 h. A transition of the radioactivity from the S2 and mitochondria fraction to the nuclear fraction was noted over the 24-h period (Fig. 10).

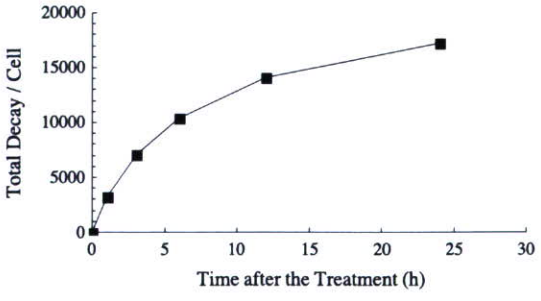

Fig. 9. Total decay frequency of intracellular ^{64}Cu. Based on the washout result shown in Fig. 8, the total decay frequency was calculated for a cell taking up a 99% cell killing dose of 1.50 Bq/cell. Radioactivity at each time point was corrected for a half-life of 12.7 h and the area under the curve was calculated.

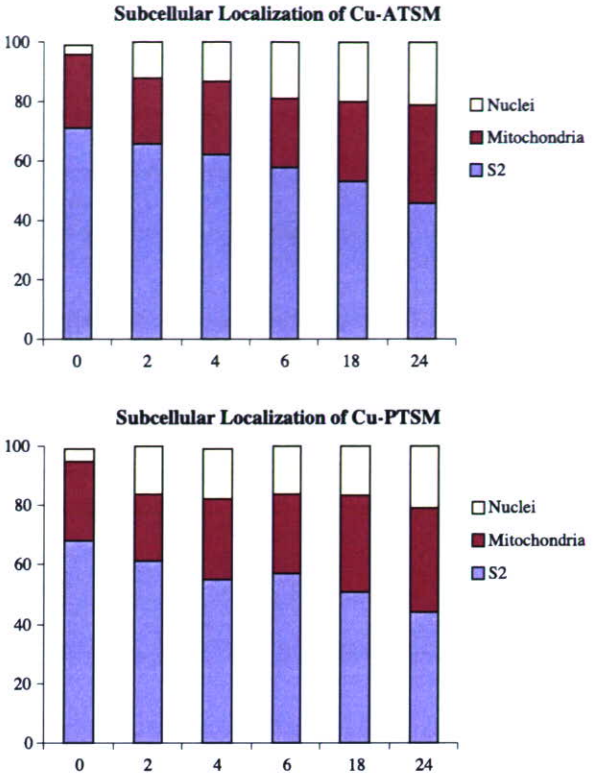

Fig. 10. Subcellular distribution of ^{64}Cu following ^{64}Cu-ATSM or ^{64}Cu-PTSM treatment. After ^{64}Cu-ATSM and ^{64}Cu-PTSM were metabolized in the cells, the majority of the ^{64}Cu was retained in the microsomal/cytosol fraction. A transition of radioactivity from the mitochondria and S2 fractions to the nuclear fractions was noted. Data are expressed as the mean percentage of total cellular radioactivity ($n=4$).

4. Discussion

^{64}Cu-ATSM has distinct accumulation mechanisms that are based on hypoxic tumor-selective metabolism by some enzymes [19]. Equipped with the radionuclidic characteristics of ^{64}Cu and the high and specific accumulation in tumor cells, ^{64}Cu-ATSM is making a new type of radiotherapy agent that provides a new strategy for the treatment of tumors [20]. In this study, we investigated the cytotoxic effect of ^{64}Cu-ATSM using clonogenic survival assays in an in vitro cell culture model. ^{64}Cu-ATSM decreased the clonogenic survival of LL/2 cells in a dose-dependent manner where 99% cell killing occurred when 1.50 Bq/cell of ^{64}Cu was taken up into the cells.

The nonligand binding form of ^{64}Cu (Cu-glycine) did not affect the survival rate of LL/2 cells, whereas the equivalent amount of radioactivity of ^{64}Cu-ATSM significantly reduced the survival rate to about 0.1% ($P<.0001$). In this experiment, the incubation medium containing ^{64}Cu was exchanged into fresh culture medium after the treatment,

meaning that the ^{64}Cu taken up into tumor cells prior to the exchange was the only source of the cell killing. The ^{64}Cu taken up into the cells was dramatically different between the ^{64}Cu-glycine-treated groups and the ^{64}Cu-ATSM-treated groups, 0.0857±0.0038 and 2.04±0.08 Bq/cell, respectively. This may be the major cause for the differences in the subsequent survival rates. Furthermore, considering that there was no difference in the survival rate between the nontreated control and ^{64}Cu-glycine groups, the radioactive emissions from outside of the cells during the 1-h treatment in the flask did not affect the tumor cell survival. To be brief, the most effective character of ^{64}Cu-ATSM is to accumulate radioactive ^{64}Cu into the cells and as such produces the ability to kill tumor cells.

Radiation causes direct and/or indirect effects on irradiated cells. One of the well-known direct effects is damage to DNA. DNA damage by ionizing radiation predominantly consists of single-strand breaks, but also includes double-strand breaks, alkali-label sites, and oxidized purines and pyrimidines [30–32]. We confirmed with the alkali comet assay that a significant increase in DNA damage was observed with ^{64}Cu-ATSM-treated groups at 6 h after treatment. Comet assay allows us to detect the DNA fragmentation in apoptotic and/or necrotic cells [33]. However, we could not detect significant increases in the number of apoptotic cells as well as necrotic and/or dead cells using the Annexin V-FITC/PI staining method at the same time point. For this reason, the DNA damage observed after the treatment was considered to be caused directly by the radiation from intracellular ^{64}Cu and not by apoptosis.

Radiation-induced DNA damage elicits a variety of cellular responses including apoptosis as one of the major mechanisms of cell death in radiation therapy [34–36]. In this study, apoptosis marker-positive cells significantly increased in number ($P<.05$) 36 h after the treatment when detected by the Annexin V-FITC/PI staining method, preceded by the inhibition of cellular proliferation 24 h after the treatment. In an X-irradiation study, high-dose irradiation was reported to induce a rapid and strong apoptotic response, whereas low-dose irradiation induced a slow and mild apoptosis; each type of apoptosis was defined as premitotic apoptosis and postmitotic apoptosis, respectively [37]. In the postmitotic apoptosis, cell death occurs after one or a few cell divisions, not immediately after the radiation, and cell cycle arrest is observed at the G_2/M phase. In our preliminary study, we also observed increase of G_2/M phase cells, namely, G_2/M arrest, in the ^{64}Cu-ATSM-treated groups at 12–24 h after the treatment. These findings indicated that the typical cell death after ^{64}Cu-ATSM treatments is through postmitotic apoptosis.

It is conceivable that ^{64}Cu-ATSM would be able to exert stronger cytotoxicity via premitotic apoptosis if a higher radiation dose of ^{64}Cu-ATSM was given to the cells. However, considering radiotherapy in clinical setting, doses should be reduced to avoid adverse effects on nontarget tissues. In this regard, the ability of ^{64}Cu-ATSM to induce mild but steady cytotoxicity and postmitotic apoptosis confirmed in this study is desirable as a radiotherapy agent.

Recently, it has been reported that the damage to DNA by ^{64}Cu might be derived from Auger electrons because about 40% of ^{64}Cu decays by electron capture emitting Auger electrons with high linear electron transfer [20]. Auger electrons are expected to bring very high toxicity if they are in close proximity to DNA. The tissue penetration range of Auger electrons emitted from ^{64}Cu is about 5 μm [20] and is shorter than the diameter of most tumor cells, so it is well recognized that the radiotoxicity of Auger electron emitters depends strongly on their distribution within the cell. The most severe effects have been observed when the Auger emitter is localized in the nucleus [38]. Therefore, also in the case of ^{64}Cu, it is necessary for the radiocopper to localize in the nucleus and around the DNA to exert cytotoxicity through Auger electrons. In this study, we investigated the subcellular distribution of ^{64}Cu after uptake into tumor cells and showed that the radioactivity existed mainly in the S2 fraction with the radioactivity slowly migrating into the nucleus over time. Furthermore, nonradioactive Cu-ATSM did not affect the survival rate, which indicated the Cu ions themselves were not cytotoxic at the concentrations used in this study. Based on these findings, β^- particles emitted from intracellular ^{64}Cu as well as the Auger emissions of ^{64}Cu in the nuclear fraction are considered to be the major cytotoxic sources in ^{64}Cu-ATSM therapies. Moreover, the maximum recoil energy from the transmutation of ^{64}Cu to its highly charged daughter nucleus may also increase the cell killing ability. The multiplicity of decay mode of ^{64}Cu seems to be working in favor of the antitumor effect of ^{64}Cu-ATSM. Previous reports showed a significant portion of ^{67}Cu-pyruvaldehyde-bis(N^4-methylthiosemicarbazone), an analog of the series of Cu(II)-bis(thiosemicarbazones) compounds, is delivered to the cell nucleus [21] and our current studies have demonstrated similar uptake patterns.

The tissue penetration range of β^- particles emitted from ^{64}Cu is up to several hundred of micrometers. For this reason, the cytotoxic effect of the β^- particle of ^{64}Cu can range not only to the single cell that take up ^{64}Cu but also to the surrounding cells that do not take up ^{64}Cu, which could increase the antitumor effect in vivo ^{64}Cu-ATSM therapy. This feature becomes important when treating in vivo tumor masses because aggregation of the cells with heterogeneous characters is expected in vivo tumors.

The washout rate of ^{64}Cu from tumor cells is relatively high in our experimental model. At 3 h after the treatment, radioactivity in the cells was reduced to 38.0% of the total uptake at the end of the treatment. However, in the biodistribution study using tumor-bearing animal models, accumulation of ^{64}Cu-ATSM into tumor cells was reported to be highest at 4 h after injection [20]. High washout rate observed in our assay system might be limited only to in vitro model and actual accumulation of ^{64}Cu in the tumor might continue for much longer periods. If so, the

therapeutic effectiveness of ^{64}Cu-ATSM might be higher in the in vivo tumors.

Based on the washout rate and half-life of ^{64}Cu, we calculated the total number of atomic disintegrations of ^{64}Cu occurring in the tumor cells when 1.50 Bq/cell of ^{64}Cu, a 99% cell killing dose, was taken up into cells (Fig. 9). Under these conditions, approximately 10,000 atomic disintegrations occurred within 6 h after the treatment, and about 14,000 within 12 h. That is, 10,000–14,000 atomic disintegrations per cell might be enough for killing tumor cells. D37 value (37% cell death) [39] was ca. 4500 decay per cell when biological washout from the cells was taken into account for the calculation, which was one fourth of the value previously reported (16,000 decay per cell) [40]. The actual area under time–radioactivity curve in the present study (Fig. 8) was about one fourth of the estimated value from nonwashout model, so that the present result is considered to be more accurate as actual retention pattern was included into the calculation.

In this study, the cells were kept under hypoxic condition during uptake phase of ^{64}Cu-ATSM to realize high retention of ^{64}Cu for 1 h, then cultured for 5 days at the maximum in normoxic condition to evaluate solely the effect of radiation, excluding the effect of hypoxia on cell viability. As hypoxia is considered to lessen the radiation toxicity in general, the cell killing ability determined in this study in normoxic tumor cells might be higher than that expected in continuously hypoxic tumor cells. On the other hand, the present results can be used for the estimation of cell toxicity in normoxic nontumor cells. Hypoxia selectivity of ^{64}Cu-ATSM is critical for realizing tumor-selective treatment. In our human studies using ^{62}Cu-ATSM, the highest accumulation was found in lung tumor (tumor/blood=3.00±1.50), followed by liver (liver/blood=2.45±1.03), whereas other normal tissues showed relatively low accumulation (heart/blood=1.84±0.35, lung/blood=0.43±0.09) [41]. High abdominal accumulation observed in mice [23] might be a result of hepatobiliary secretion of ^{64}Cu after metabolism. From these findings, cytotoxicity in the liver and, to a lesser extent, in the intestine arise as a possible problem in ^{64}Cu-ATSM treatment. Roughly 75% of the blood entering the liver is from portal vein and 25% from hepatic artery. Thus, considerable part of the liver seems to be hypoxic and it might be responsible for the rather high uptake of ^{64}Cu-ATSM in the liver. If so, radiation effect of ^{64}Cu in the liver could be estimated in a similar manner as in hypoxic tumor cells. Physiological excretion route of Cu is from liver to duodenum. Radioactive ^{64}Cu injected as Cu-ATSM is also expected to follow this route after released from the chelate. As shown in the present study, extracellular ^{64}Cu did not show significant cell toxicity, so that radioactivity in the duodenum is less likely to become a source of adverse effect in the treatment.

In vitro cell uptake study reported previously, Cu-ATSM showed some uptake also in normoxic tumor cells [23]. However, in our PET studies in normal human, selective Cu accumulation was found only in the liver but no other tissues (unpublished data). Thus, the uptake in the normoxic tumor cells might be from a characteristic of tumor cells. In fact, tumor cells expressed microsomal electron transport enzymes and they played a major role in reductive retention of Cu-ATSM in tumor cells, especially under hypoxic conditions [19]. Thus, Cu-ATSM can be evaluated mainly as a marker of hypoxia and, in some part, as a marker of tumor-selective gene expression by means of microsomal enzyme expression, in clinical practice.

5. Conclusion

^{64}Cu-ATSM has been shown to be effective in the treatment of tumors. ^{64}Cu-ATSM efficiently delivered radioactive ^{64}Cu into hypoxic tumor cells and the emitted β^- particles caused lethal damage to DNA leading to postmitotic apoptosis and mild but steady cell death. Since Cu-ATSM showed low but considerable uptake in normoxic cells in vitro and may be taken up in normoxic cells in vivo, the therapeutic index need to be carefully considered. In order to ensure the safety and effectiveness of ^{64}Cu-ATSM treatment, contribution of hypoxia on both ^{64}Cu accumulation and radiation sensitivity of target and/or nontarget cells and possible adverse effects to the excretion route should be clarified.

Acknowledgments

Part of this study is supported by a Grant-in-Aid for Scientific Research (Kakenhi No. 1430274) from JSPS, Research and Development Project Aimed at Economic Revitalization from the Ministery of Education, Culture, Science, Sports and Technology Japan, and the 21st Century COE program "Biomedical Imaging Technology Integration Program" from JSPS.

The production of Cu-64 at Washington University is supported by NCI R24 CA86307. Additional financial support for the studies at Washington University came from the United States Department of Energy grant (DE-FG02-87ER60212).

References

[1] Zuckier LS, DeNardo GL. Trials and tribulations: oncological antibody imaging comes to the fore. Semin Nucl Med 1997;27(1): 10–29.

[2] Burke JM, Jurcic JG, Scheinberg DA. Radioimmunotherapy for acute leukemia. Cancer Control 2002;9(2):106–13.

[3] Frankel AE, Sievers EL, Scheinberg DA. Cell surface receptor-targeted therapy of acute myeloid leukemia: a review. Cancer Biother Radiopharm 2000;15(5):459–76.

[4] Postema EJ, Boerman OC, Oyen WJ, Raemaekers JM, Corstens FH. Radioimmunotherapy of B-cell non-Hodgkin's lymphoma. Eur J Nucl Med 2001;28(11):1725–35.

[5] Burke PA, DeNardo SJ, Miers LA, Kukis DL, DeNardo GL. Combined modality radioimmunotherapy. Promise and peril. Cancer 2002;94(4 Suppl):1320–31.

[6] Choy H, Akerley W, Glantz M, Safran H, Graziano S, Chung C. Concurrent paclitaxel and radiation therapy for solid tumors. Cancer Control 1996;3(4):310–8.
[7] Colcher D, Bird R, Roselli M, Hardman KD, Johnson S, Pope S, et al. In vivo tumor targeting of a recombinant single-chain antigen-binding protein. J Natl Cancer Inst 1990;82(14):1191–7.
[8] Smyth MJ, Pietersz GA, McKenzie IF. Use of vasoactive agents to increase tumor perfusion and the antitumor efficacy of drug-monoclonal antibody conjugates. J Natl Cancer Inst 1987;79(6):1367–73.
[9] Delaloye AB, Delaloye B, Buchegger F, Vogel CA, Gillet M, Mach JP, et al. Comparison of copper-67- and iodine-125-labeled anti-CEA monoclonal antibody biodistribution in patients with colorectal tumors. J Nucl Med 1997;38(6):847–53.
[10] Kroger LA, DeNardo GL, Gumerlock PH, Xiong CY, Winthrop MD, Shi XB, et al. Apoptosis-related gene and protein expression in human lymphoma xenografts (Raji) after low dose rate radiation using ^{67}Cu-2IT-BAT-Lym-1 radioimmunotherapy. Cancer Biother Radiopharm 2001;16(3):213–25.
[11] Anderson CJ, Schwarz SW, Connett JM, Cutler PD, Guo LW, Germain CJ, et al. Preparation, biodistribution and dosimetry of copper-64-labeled anti-colorectal carcinoma monoclonal antibody fragments 1A3-F(ab′)2. J Nucl Med 1995;36(5):850–8.
[12] Lewis JS, Lewis MR, Cutler PD, Srinivasan A, Schmidt MA, Schwarz SW, et al. Radiotherapy and dosimetry of ^{64}Cu-TETA-Tyr3-octreotate in a somatostatin receptor-positive, tumor-bearing rat model. Clin Cancer Res 1999;5(11):3608–16.
[13] Apelgot S, Coppey J, Gaudemer A, Grisvard J, Guille E, Sasaki I, et al. Similar lethal effect in mammalian cells for two radioisotopes of copper with different decay schemes, ^{64}Cu and ^{67}Cu. Int J Radiat Biol 1989;55(3):365–84.
[14] Connett JM, Anderson CJ, Guo LW, Schwarz SW, Zinn KR, Rogers BE, et al. Radioimmunotherapy with a ^{64}Cu-labeled monoclonal antibody: a comparison with ^{67}Cu. Proc Natl Acad Sci U S A 1996; 93(13):6814–8.
[15] McCarthy DW, Shefer RE, Klinkowstein RE, Bass LA, Margeneau WH, Cutler CS, et al. Efficient production of high specific activity ^{64}Cu using a biomedical cyclotron. Nucl Med Biol 1997;24(1):35–43.
[16] Obata A, Kasamatsu S, McCarthy DW, Welch MJ, Saji H, Yonekura Y, et al. Production of therapeutic quantities of ^{64}Cu using a 12 MeV cyclotron. Nucl Med Biol 2003;30(5):535–9.
[17] Fujibayashi Y, Cutler CS, Anderson CJ, McCarthy DW, Jones LA, Sharp T, et al. Comparative studies of Cu-64-ATSM and C-11-acetate in an acute myocardial infarction model: ex vivo imaging of hypoxia in rats. Nucl Med Biol 1999;26(1):117–21.
[18] Fujibayashi Y, Taniuchi H, Yonekura Y, Ohtani H, Konishi J, Yokoyama A. Copper-62-ATSM: a new hypoxia imaging agent with high membrane permeability and low redox potential. J Nucl Med 1997;38(7):1155–60.
[19] Obata A, Yoshimi E, Waki A, Lewis JS, Oyama N, Welch MJ, et al. Retention mechanism of hypoxia selective nuclear imaging/radiotherapeutic agent Cu-diacetyl-bis(N^4-methylthiosemicarbazone) (Cu-ATSM) in tumor cells. Ann Nucl Med 2001;15(6):499–504.
[20] Lewis J, Laforest R, Buettner T, Song S, Fujibayashi Y, Connett J, et al. Copper-64-diacetyl-bis(N^4-methylthiosemicarbazone): an agent for radiotherapy. Proc Natl Acad Sci U S A 2001;98(3):1206–11.
[21] Baerga ID, Maickel RP, Green MA. Subcellular distribution of tissue radiocopper following intravenous administration of ^{67}Cu-labeled Cu-PTSM. Int J Radiat Appl Instrum B 1992;19(6):697–701.
[22] Gingras BA, Suprunchuk T, Bayley CH. The preparation of some thiosemicarbazones and their copper complexes. Can J Chem 1962; 40:1053–9.
[23] Lewis JS, McCarthy DW, McCarthy TJ, Fujibayashi Y, Welch MJ. Evaluation of ^{64}Cu-ATSM in vitro and in vivo in a hypoxic tumor model. J Nucl Med 1999;40(1):177–83.
[24] Rao GS, Murray S, Ethier SP. Radiosensitization of human breast cancer cells by a novel ErbB family receptor tyrosine kinase inhibitor. Int J Radiat Oncol Biol Phys 2000;48(5):1519–28.
[25] Rockwell S. In vivo–in vitro tumor systems: new models for studying the response of tumors to therapy. Lab Anim Sci 1977;27:813–51.
[26] Rojas E, Lopez MC, Valverde M. Single cell gel electrophoresis assay: methodology and applications. J Chromatogr, B Biomed Sci Appl 1999;722:225–54.
[27] Swart JM, Chiles TC. Rescue of CH31 B cells from antigen receptor-induced apoptosis by inhibition of p38 MAPK. Biochem Biophys Res Commun 2000;276(2):417–21.
[28] Hertveldt K, Philippe J, Thierens H, Cornelissen M, Vral A, De Ridder L. Flow cytometry as a quantitative and sensitive method to evaluate low dose radiation induced apoptosis in vitro in human peripheral blood lymphocytes. Int J Radiat Biol 1997;71(4):429–33.
[29] Vermes I, Haanen C, Steffens-Nakken H, Reutelingsperger C. A novel assay for apoptosis. Flow cytometric detection of phosphatidylserine expression on early apoptotic cells using fluorescein labelled Annexin V. J Immunol Methods 1995;184(1):39–51.
[30] Frankenberg-Schwager M. Induction, repair and biological relevance of radiation-induced DNA legions in eukaryotic cells. Radiat Environ Biophys 1990;29:273–92.
[31] Goodhead DT. Initial events in the cellular effects of ionizing radiations: clustered damage in DNA. Int J Radiat Biol 1994;65(1): 7–17.
[32] Ward JF. Radiation mutagenesis: the initial DNA lesions responsible. Radiat Res 1995;142(3):362–8.
[33] Godard T, Deslandes E, Lebailly P, Vigreux C, Sichel F, Poul JM, et al. Early detection of staurosporine-induced apoptosis by comet and annexin V assays. Histochem Cell Biol 1999;112(2):155–61.
[34] Knox SJ, Sutherland W, Goris ML. Correlation of tumor sensitivity to low-dose-rate irradiation with G2/M-phase block and other radiobiological parameters. Radiat Res 1993;135(1):24–31.
[35] Kroger LA, DeNardo SJ, DeNardo GL, Xiong CY, Winthrop MD, Gumerlock PH. Effect of ^{67}Cu-2IT-BAT-Lym-1 therapy on BCL-2 gene and protein expression in a lymphoma mouse model. Clin Cancer Res 1999;5(10 Suppl):3010s–4s.
[36] Macklis RM, Beresford BA, Palayoor S, Sweeney S, Humm JL. Cell cycle alterations, apoptosis, and response to low-dose-rate radioimmunotherapy in lymphoma cells. Int J Radiat Oncol Biol Phys 1993;27(3):643–50.
[37] Shinomiya N, Kuno Y, Yamamoto F, Fukasawa M, Okumura A, Uefuji M, et al. Different mechanisms between premitotic apoptosis and postmitotic apoptosis in X-irradiated U937 cells. Int J Radiat Oncol Biol Phys 2000;47(3):767–77.
[38] Hofer KG, Harris CR, Smith M. Radiotoxicity of intracellular Ga-67, I-125 and H-3. Nuclear versus cytoplasmic radiation effects in murine L1210 leukaemia. Int J Radiat Biol Relat Stud Phys Chem Med 1975;28:225–41.
[39] Hall EJ. The shape of the survival curve. In: Hall EJ, editor. Radiobiology for the radiologist. Philadelphia: J.B. Lippincott Co; 1994. p. 32–9.
[40] Anderson CJ, Connett JM, Baumann ML, Schwarz SW, Zinn KR, Phlipott GW, et al. Comparison of Cu-67 and Cu-64 as potential radionuclides for radiotherapy. J Nucl Med 1993;34(5):134P.
[41] Takahashi N, Fujibayashi Y, Yonekura Y, Welch MJ, Waki A, Tsuchida T, et al. Evaluation of ^{62}Cu labeled diacetyl-bis(N^4-methylthiosemicarbazone) as a hypoxic tissue tracer in patients with lung cancer. Ann Nucl Med 2000;14(5):323–8.

Enhanced Apoptotic Reaction Correlates with Suppressed Tumor Glucose Utilization After Cytotoxic Chemotherapy: Use of ^{99m}Tc-Annexin V, ^{18}F-FDG, and Histologic Evaluation

Toshiki Takei, MD[1]; Yuji Kuge, PhD[2]; Songji Zhao, MD[2]; Masayuki Sato, BS[3]; H. William Strauss, MD[4]; Francis G. Blankenberg, MD[5]; Jonathan F. Tait, MD, PhD[6]; and Nagara Tamaki, MD[1]

[1]Department of Nuclear Medicine, Graduate School of Medicine, Hokkaido University, Sapporo, Japan; [2]Department of Tracer Kinetics, Graduate School of Medicine, Hokkaido University, Sapporo, Japan; [3]Department of Radiopharmaceutical Chemistry, Health Sciences University of Hokkaido, Tobetsu, Japan; [4]Department of Nuclear Medicine, Memorial Sloan–Kettering Cancer Center, New York, New York; [5]Division of Nuclear Medicine, Department of Radiology, Stanford University School of Medicine, Stanford, California; and [6]Department of Laboratory Medicine, University of Washington, Seattle, Washington

Cancer chemotherapy enhances the apoptosis, whereas apoptosis is a suicidal mechanism requiring energy. We determined the relationship between apoptosis and glucose utilization during cancer chemotherapy using ^{99m}Tc-annexin V (^{99m}Tc-annexin A5) and ^{18}F-FDG and compared their uptake with histologic findings in a rat tumor model. **Methods:** Allogenic hepatoma cells (KDH-8) were inoculated into the left calf muscle of male Wistar rats (WKA). Eleven days after the inoculation, the rats were randomly divided into 3 groups: The first group (n = 7) received a single dose of gemcitabine (90 mg/kg, intravenously), the second group (n = 8) received cyclophosphamide (150 mg/kg, intraperitoneally), and the third group (n = 7) was untreated and served as the control group. We injected ^{99m}Tc-annexin V 48 h after the chemotherapy and then injected ^{18}F-FDG to all rats 1 h before sacrifice. Six hours after ^{99m}Tc-annexin V injection, the rats were sacrificed and the organs, including the tumor, were removed and radioactivity was counted. The radioactivities of ^{18}F and ^{99m}Tc in the organs were determined using normalization by tissue weight. Histologic evaluation by the terminal deoxynucleotidyl transferase-mediated deoxyuridine triphosphate nick-end labeling (TUNEL) method and the immunostaining of glucose transporter-1 (GLUT-1) were also performed to obtain the indices of apoptosis and glucose utilization, respectively. The rate of positively stained cells was calculated and analyzed statistically. **Results:** After chemotherapy using gemcitabine and cyclophosphamide, the ^{99m}Tc-annexin V uptake (percentage injected dose per gram × kg [(%ID/g) × kg]; mean ± SD) in tumor increased significantly (0.062 ± 0.012 (%ID/g) × kg in the gemcitabine-treated group and 0.050 ± 0.012 (%ID/g) × kg in the cyclophosphamide group vs. 0.031 ± 0.005 (%ID/g) × kg in the control group; $P < 0.01$). In contrast, the ^{18}F-FDG in tumor decreased significantly (0.483 ± 0.118 (%ID/g) × kg in the gemcitabine group and 0.583 ± 0.142 (%ID/g) × kg in the cyclophosphamide group) compared with that in the control group (0.743 ± 0.084 (%ID/g) × kg; $P < 0.01$). In addition, ^{18}F-FDG uptake in tumor negatively correlated with ^{99m}Tc-annexin V uptake ($r = -0.75$; $P < 0.01$). In the gemcitabine and cyclophosphamide groups, the rate of TUNEL positively stained cells was significantly higher than that in the control group (10.2% ± 1.7% and 8.0% ± 1.5% vs. 5.2% ± 1.5%; $P < 0.01$), whereas the GLUT-1 expression level showed no definite changes in histologic analyses. **Conclusion:** These data indicate that an enhanced apoptotic reaction correlated with suppressed tumor glucose utilization after cytotoxic chemotherapy as determined using radiotracers and histologic evaluation. The increase in ^{99m}Tc-annexin V and the decrease in ^{18}F-FDG in tumor can be useful markers for predicting therapeutic outcomes and for prognosis at the early stage of chemotherapy.

Key Words: molecular imaging; ^{18}F-FDG; ^{99m}Tc-annexin V; apoptosis; cancer chemotherapy

J Nucl Med 2005; 46:794–799

Apoptosis, or programmed cell death, is activated in the course of successful antineoplastic therapy (*1–3*). Determining baseline levels of apoptosis and the increment of apoptosis induced by therapy can serve as useful prognostic markers (*4,5*). Cancer chemotherapy with agents such as 2′,2′-difluoro-2′-deoxycytidine (gemcitabine) and cyclophosphamide not only arrest metabolism and induce DNA alkylation, respectively, but also enhance apoptosis (*6,7*). Early in the course of apoptosis, phosphatidylserine (PS) is expressed on the external leaflet of the cell membrane. Annexin V (annexin A5), a human protein with a high affinity for membrane-bound PS, can be labeled with ^{99m}Tc for in vivo imaging of apoptosis (*8*). In an earlier study, we used this imaging technique to quantify the time course and

Received Sep. 11, 2004; revision accepted Dec. 8, 2004.

For correspondence or reprints contact: Nagara Tamaki, MD, Department of Nuclear Medicine, Graduate School of Medicine, Hokkaido, University, Kita 15 Nishi 7, Kita-ku, Sapporo 060-8638, Japan.
E-mail: natamaki@med.hokudai.ac.jp

intensity of apoptosis induced by treatment with cyclophosphamide (*7,9,10*).

Because apoptosis requires energy to destroy cellular DNA and produce apoptosomes, evaluating cellular metabolism in the course of apoptosis may identify the process with an increase in substrate consumption. Since glucose is a major substrate for tumor cells, serial images recorded with the glucose analog ^{18}F-FDG may be useful for this purpose. Although ^{18}F-FDG PET is widely applied for clinical staging, differential diagnosis, therapy monitoring, detecting recurrence, and prognostic prediction of malignant diseases (*11,12*), clinical studies typically demonstrate a decrease in ^{18}F-FDG uptake before morphologic regression after appropriate chemotherapeutic regimens. Furthermore, the degree of initial metabolic suppression by chemotherapy can be correlated with the therapeutic outcomes such as malignant lymphoma or head and neck cancer (*13,14*).

This study was undertaken to compare the apoptotic response with the metabolic response in animals with implanted hepatomas and to determine the relative sensitivity of each approach to identify successful treatment.

MATERIALS AND METHODS

Preparation of Animal Models

All procedures involving animals were performed in accordance with institutional guidelines (Guide for the Care and Use of Laboratory Animals of Hokkaido University). KDH-8 is a rat transplantable hepatocellular carcinoma induced by 3′-methyl-4-dimethylaminoazobenzene in Wistar King Aptekman/Hok (WKA/H) rats (supplied by the Experimental Animal Institute, Graduate School of Medicine, Hokkaido University, Sapporo) and maintained in vivo by intraperitoneal passage every 5 d (supplied by the Department of Pathologic Oncology, Graduate School of Medicine, Hokkaido University, Sapporo). KDH-8 rat allogenic hepatoma cells (1×10^6 cells per rat) were inoculated into the left calf muscle of 8-wk-old male WKA/H rats (*7,15*). No obvious rejection or graft-versus-host reaction was observed. Our previous study showed a high uptake of ^{18}F-FDG and high expression of GLUT-1 in this KDH-8 rat tumor (*16*). Cyclophosphamide (Endoxan; Baxter) and gemcitabine (GEMZAR; Eli Lilly) were each dissolved in saline for injection. Eleven days after the intramuscular injection of KDH-8 tumor cells, rats, which weighed 187–253 g (measuring about 15 mm in diameter), with palpable tumors were randomly divided into 3 groups. The first group (n = 7) was treated with a single dose of gemcitabine (90 mg/kg, intravenously), the second group (n = 8) was treated with a single dose of cyclophosphamide (150 mg/kg, intraperitoneally), and the third group (n = 7) was untreated (control group) (*7,17*). All rats were anesthetized with pentobarbital (0.025 mg/kg, intraperitoneally) when these treatments were undertaken.

Methods Using Radioactive Tracers and Determining Biodistribution

Human annexin V was produced by expression in *Escherichia coli* as described (*8,18–21*). Annexin V was derivatized with hydrazinonicotinamide (HYNIC) and then labeled with ^{99m}Tc with tricine as coligand as described (*8*) to a specific activity of 3.0 MBq/μg protein. Rats were fasted overnight before sacrifice. ^{99m}Tc-Annexin V (37 MBq) was injected intravenously approximately 48 h after chemotherapy. The animals were under pentobarbital anesthesia at the time of radiopharmaceutical injection. One hour before sacrifice, 20 MBq of ^{18}F-FDG were injected intravenously. The radiopharmaceuticals were injected intravenously into the coccygeal vein. The blood sugar level was measured immediately before ^{18}F-FDG injection (BS1) and immediately before sacrifice (BS2). Six hours after the ^{99m}Tc-annexin V injection (1 h after ^{18}F-FDG injection), the rats were sacrificed by whole-blood sampling under ether inhalation anesthesia. The tumor, an aliquot of blood, and the contralateral femoral muscle were removed, cleaned, and weighed; radioactivity was determined using an automatic γ-counter (1480 WIZARDTM3″; Wallac Co., Ltd.). First, ^{18}F activity was measured (energy peak, 511 keV ± 20%). After >24 h for decay of ^{18}F, ^{99m}Tc activity was determined (energy peak, 140 keV ± 20%). A time-line diagram of this study is shown in Figure 1.

Activity in each window was compared with an aliquot of the injected dose to permit calculation of percentage uptake/gram of tissue after normalization to the rat's weight ((%ID/g) × kg). The tumor samples were divided into 3 parts. Using aliquots of the tumor tissues, formalin-fixed, paraffin-embedded specimens then were prepared for subsequent histologic studies. The tumor-to-muscle ratio (T/M ratio) and the tumor-to-blood ratio (T/B ratio) were calculated from the (%ID/g) × kg value in each tissue (*7,10,15*).

Histologic Evaluation

Apoptotic cells were determined by hematoxylin and eosin staining and the direct immunoperoxidase detection of digoxigenin-labeled 3′ DNA strand breaks by the use of the terminal deoxynucleotidyl transferase-mediated deoxyuridine triphosphate nick-end labeling (TUNEL) method. The formalin-fixed, paraffin-embedded tissues were sectioned at 3-μm thickness. TUNEL was performed according to a standard procedure using a commercially available kit (Apoptosis in situ Detection Kit; Wako Pure Chemical Industries, Ltd.).

The expression of glucose transporter-1 (GLUT-1) in adjacent slices was examined according to a standard immunostaining

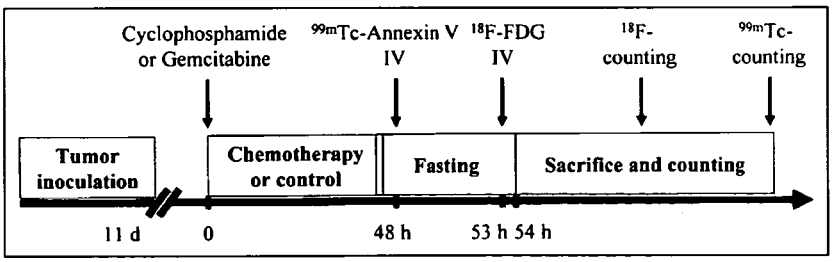

FIGURE 1. Time-line diagram of this study. IV = intravenously.

procedure. Deparaffinized sections were incubated with an anti–GLUT-1 antibody (Chemicon International, Inc.) at 37°C. The bound antibody was visualized using the avidin/biotin conjugate immunoperoxidase procedure with a HISTOFINE SAB-PO kit (Nichirei) and 3,3′-diaminobenzine tetrahydrochloride.

TUNEL and GLUT-1 positively stained cells were counted in 10 randomly selected high-power (×200) fields (with no knowledge of the treatment to avoid experimental bias) (*7,10,15*). The rate of TUNEL positively stained cells was determined by calculating the average percentage. The expression level of GLUT-1 was assessed semiquantitatively by the product of scores estimated (intensity × % positivity) according to our previous reports (*16,22*). The intensity of staining was graded (intensity) from 0 to 3 (0, not stained; 1, equivocal; 2, intense staining; and 3, very intense staining) and the percentage of positively stained cells (% positivity) was scored from 1 to 5 (1, 0%–20%; 2, 21%–40%; 3, 41%–60%; 4, 61%–80%; and 5, 81%–100%). The mean values of these levels were determined as immunohistologic GLUT-1 expression level.

Statistical Analysis

All values are shown as mean ± SD. Statistical analyses were performed using an unpaired Student *t* test to evaluate the significance of differences in values between the control and treated rats (*7,10*). Simple regression analysis was performed to compare the uptake of ^{99m}Tc-annexin V and that of ^{18}F-FDG. A 2-tailed value of $P < 0.05$ was considered significant.

RESULTS

Determination of Apoptosis

The uptake of ^{99m}Tc-annexin V in tumor tissue after gemcitabine and cyclophosphamide treatment was 0.062 ± 0.012 and 0.050 ± 0.012 (%ID/g) × kg, respectively (Table 1). The uptake of ^{99m}Tc-annexin V in tumor in both treated groups was significantly higher than that in the control group (0.031 ± 0.005 (%ID/g) × kg; $P < 0.01$). Two of the radiopharmaceuticals' uptakes in blood and muscle were not altered significantly by the 2 kinds of chemotherapeutic treatments. The TBRs of ^{99m}Tc-annexin V were 2.021 ± 0.323, 2.482 ± 0.407, and 1.414 ± 0.082 and the TMRs of ^{99m}Tc-annexin V were 7.283 ± 1.632, 7.095 ± 1.328, and 4.497 ± 0.824 in the gemcitabine-treated, cyclophosphamide-treated, and control groups, respectively. Both TBR and TMR in the treated groups were also significantly higher than those in the control group ($P < 0.01$).

In the gemcitabine-treated, cyclophosphamide-treated, and control groups, the rate of TUNEL positively stained cells were 10.2% ± 1.7%, 8.0% ± 1.5%, and 5.2% ± 1.5%, respectively. These apoptotic rates also increased in both treatment groups (Table 1).

Determination of Glucose Utilization

The uptake of ^{18}F-FDG in tumor tissue after gemcitabine and cyclophosphamide treatment was 0.483 ± 0.118 and 0.583 ± 0.142 (%ID/g) × kg, respectively (Table 2). The uptake of ^{18}F-FDG in tumor in both treated groups was significantly lower than that in the control group (0.743 ± 0.084 (%ID/g) × kg; $P < 0.01$). The TBRs of ^{18}F-FDG were 9.885 ± 4.592, 12.21 ± 7.145, and 15.21 ± 1.487 and the TMRs of ^{18}F-FDG were 15.15 ± 6.062, 7.859 ± 4.464, and 33.44 ± 4.721 in the gemcitabine-treated, cyclophosphamide-treated, and control groups, respectively. Both the TBRs and TMRs in the treated groups were also significantly lower than those in the control group ($P < 0.05$).

The expression levels of GLUT-1 estimated on the basis of positivity (intensity × percentage) were 58.3 ± 4.9, 61.1 ± 6.9, and 60.5 ± 5.6 in the gemcitabine-treated, cyclophosphamide-treated, and control groups, respectively. Although all 3 groups showed very high expression levels in the cancer cells, there was no statistically significant difference in the expression level of GLUT-1 between treated and control tissues (Table 2).

Relationship Between Uptake of ^{99m}Tc-Annexin V and ^{18}F-FDG in Tumor

Figure 2 shows a scattergram of the uptake of ^{99m}Tc-annexin V and ^{18}F-FDG in tumor. ^{18}F-FDG uptake in tumor showed a significantly negative correlation with that of ^{99m}Tc-annexin V uptake ($r = -0.75$; $P < 0.01$).

Blood Glucose Level and Tumor Weight

The tumor weights were 3.239 ± 1.520, 4.168 ± 2.007, and 3.503 ± 1.145 g in the gemcitabine-treated, cyclophosphamide-treated, and control groups, respectively. The blood glucose levels at BS1 was 114.1 ± 13.01, 118.9 ±

TABLE 1
Apoptotic Indices According to Uptake of ^{99m}Tc-Annexin V and Rate of TUNEL Positively Stained Cells

Parameter	Control	Gemcitabine	Cyclophosphamide
Tumor uptake (%ID/g) × kg	0.031 ± 0.005	0.062 ± 0.012*	0.050 ± 0.012*
Blood uptake (%ID/g) × kg	0.022 ± 0.002	0.024 ± 0.004*	0.025 ± 0.004*
Muscle uptake (%ID/g) × kg	0.007 ± 0.002	0.007 ± 0.003*	0.009 ± 0.002*
T/B ratio	1.414 ± 0.082	2.021 ± 0.323*	2.482 ± 0.407*
T/M ratio	4.497 ± 0.824	7.283 ± 1.632*	7.095 ± 1.328*
TUNEL positive (%)	5.2 ± 1.5	10.2 ± 1.7*	8.0 ± 1.5*

*$P < 0.01$ compared with control group.
Data are mean ± SD.